LAMINAR FLOW DEVELOPMENT DOWNSTREAM OF AN ABRUPT CIRCULAR CHANNEL EXPANSION

LAMINAR FLOW DEVELOPMENT DOWNSTREAM OF AN ABRUPT CIRCULAR CHANNEL EXPANSION

BY

GRAHAM K. PIKE B. Eng.

A THESIS

SUBMITTED TO THE FACULTY OF GRADUATE STUDIES

IN PARTIAL FULFILMENT OF THE REQUIREMENTS

for the degree

MASTER OF ENGINEERING

McMaster University

June 1973

© Graham K. Pike 1974

MASTER OF ENGINEERING (1973)
(Mechanical Engineering)

McMaster University
Hamilton, Ontario

TITLE: Laminar Flow Development Downstream of an Abrupt Circular Channel Expansion

AUTHOR: Graham K. Pike

SUPERVISORS: Dr. G. F. Round, Dr. I. A. Feuerstein

NUMBER OF PAGES: X, 100

ABSTRACT

This dissertation reports the development of a flow visualisation technique which was used to study the flow pattern generated by an abrupt expansion in a circular section conduit, Experiments were performed at Reynolds numbers (based on upstream tube diameter) ranging from 222 to 755 and for tube diameter ratios of 0.63, 0.79 and 0.93.

Velocity profiles were obtained at each of two different stations beyond the vortex and these were used as upstream boundary conditions for the linearized axial Navier-Stokes equation for the purpose of predicting development lengths. A correlation was obtained for development length as follows:

$$L/D = 0.27\ Re_D^{0.94}\ [\ 1 - (d/D)^{2.77}\ ]$$

Measurements of vortex length were made for a tube diameter ratio of 0.63 and the results correlated in the form

$$x_R/h = 0.048\ Re_d^{1.1}$$

Hence both vortex length and development length increase almost linearly with Reynolds number.

ACKNOWLEDGEMENTS

The author expresses his gratitude to Dr. G. F. Round, Chairman, Department of Mechanical Engineering and to Dr. I. A. Feuerstein, Department of Chemical Engineering, for their invaluable advice and constant encouragement throughout this work. Appreciation is also expressed for the help given by the Chemical Engineering Departmental Technicians in constructing much of the experimental equipment.

TABLE OF CONTENTS

CHAPTER		PAGE
	List of Tables	VI
	List of Figures	VII
	List of Plates	VIII
	Nomenclature	IX
1	INTRODUCTION	1
	1.1 General	1
	1.2 The Vortex Region	1
	1.3 Flow Regimes at Higher Reynolds Numbers	3
	1.4 Flow Development in the Laminar Regime	3
2	THEORY	4
3	DESCRIPTION OF APPARATUS	10
	3.1 Flow System	10
	3.2 Optical Equipment	20
4	EXPERIMENTAL PROCEDURE	30
5	RESULTS AND DISCUSSION	36
	5.1 Flow Development	36
	5.2 The Vortex Region	59
6	CONCLUSIONS	62
	REFERENCES	64
APPENDIX		
1	Particle Inertia Effects	66
2	The Solution to Equation 2.10	70

APPENDIX		PAGE
3	Derivation of an Expression for ϵ	74
4	Estimation of Displacement of Particle Image due to Refraction of Bounding Rays at Liquid/Glass Interface	77
5	Error Analysis	79
6	Computer Programme	81
7	Tabulated Experimental Data	92

LIST OF TABLES

TABLE NO.		PAGE
1	Composition and Properties of Suspending Fluid	13
2	Dimensions of Glass Tubes	17
3-10	Velocity Data for Experiments A1 to C3	92-100
11	Reynolds Numbers Based on Upstream and Downstream Tube Diameters	47
12	Non-Dimensional Form of Velocity Profile and Maximum Value of Z	48
13	Development Lengths	55

LIST OF FIGURES

FIGURE NO.		PAGE
1	Schematic Diagram of Flow System	11
2	Viscosity - Temperature Curve for Suspending Fluid	14
3	Teflon Expansion Piece	16
4	Mixing Chamber	18
5	Aluminium Venturimeter	21
6	Venturimeter Calibration Curve	22
7	Hycam Speed Curves	29
8	Film Analysis	34
9	Experimental Notation	37
10 - 17	Experimentally Determined Velocity Profiles	38-45
18	Mathematically Generated Sequence of Velocity Profiles with Decreasing Centreline Velocity	52
19	Mathematically Generated Sequence of Velocity Profiles with Increasing Centreline Velocity	53
20	Stretching Factor, ϵ, Verus Stretched Coordinate, Z^*, for Curves of Figures 18 and 19	54
21	Reattachment Length Versus Upstream Reynolds Number for a Tube Diameter Ratio of 0.63	60

LIST OF PLATES

PLATE NO.		PAGE
1	Viewing Cell	23
2	Front Surface Reflecting Mirror in Brass Mount	25
3	Side View of High Speed Movie Camera and Viewing Cell	27
4	Sequence of 20 Frames from 16mm. Film	35

NOMENCLATURE

DIMENSIONAL

r	radial coordinate
z	axial coordinate
V_m	mean fluid velocity
v_r	radial velocity component
v_z	axial velocity component
$(v_z)_{fd}$	fully developed velocity
g_z	axial component of gravitational acceleration
p	static pressure
q, Q	flowrate
ρ	density
μ	dynamic viscosity
ν	kinematic viscosity
A	cross-sectional area of larger diameter tube
h	step height at expansion
R	radius of larger tube

NON-DIMENSIONAL

d/D	tube diameter ratio (≤ 1)
P	particle to tube diameter ratio
Re_d, Re_D	Reynolds Numbers based on mean fluid velocity
η	non-dimensional radial coordinate, r/R
ω	non-dimensional axial velocity, v_z/V_m

Z	non-dimensional axial parameter, $(z/R) / (V_m R/\nu)$

MATHEMATICAL

α, β	Functions of axial coordinate, Z, which appear in Langhaar's solution
ϵ, Λ	Functions of Z which appear in the solution of Sparrow et. al.
D/Dt	Total Differential
∇^2	Laplacian Operator
$J_N(x)$	Bessel Function of First Kind of Order N
$Y_N(x)$	Bessel Function of Second Kind of Order N

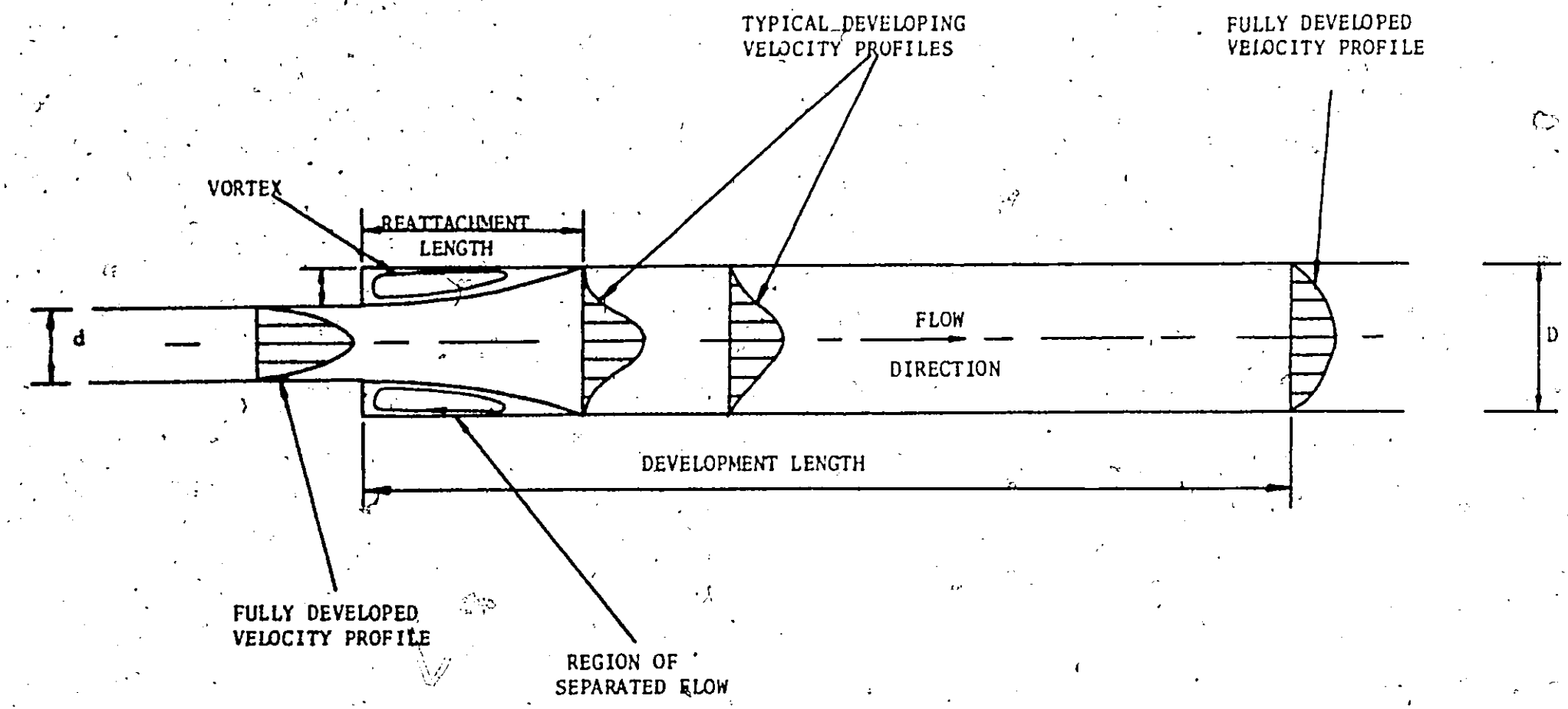
TYPICAL DEVELOPING
VELOCITY PROFILES
FULLY DEVELOPED
VELOCITY PROFILE
VORTEX
REATTACHMENT
LENGTH
d
FLOW
DIRECTION
D
DEVELOPMENT LENGTH
FULLY DEVELOPED
VELOCITY PROFILE
REGION OF
SEPARATED FLOW

1. INTRODUCTION

1.1 General

The primary object of this work has been the development of a simple flow visualisation technique in which the flow pattern is revealed by the presence of small, neutrally buoyant tracer particles. It is then possible to obtain reasonably accurate quantitative data with theaid of a high-speed movie camera. This technique should be particularly useful for revealing secondary flow patterns in more complicated geometries such as a three-dimensional bifurcation. The latter geometry is of special interest in biological work in connection with studies of the circulation in the cardiovascular system and of the flow of air in the respiratory tracts.

Because of its geometrical simplicity, the abrupt, circular channel expansion is ideally suited as a model for illustrating the above method. Further, although numerical solutions have been obtained for the governing equations, there appears as yet to be no information in the literature concerning flow development beyond the step and no values have been presented for development length.

1.2 The Vortex Region

The flow pattern generated by an axisymmetric step expansion in a circular conduit may be visualised as consisting of a separated region of circulatory flow separated from that of the mainstream and held captive between it and the tube walls. Macagno and Hung (1) have analysed the dynamic interaction between the annular vortex and the sustaining flow for a tube

diameter ratio of 0.5 and for upstream Reynolds numbers (based on tube diameter and mean velocity) of up to 200. It appears from their investigation that the main role of the vortex is that of helping to shape the main flow with very little exchange of energy between the two.

Measurements of vortex length and position of the centre of rotation obtained from photographic records and by direct observation of dye filaments indicate a linear increase of both quantities with Reynolds number, with a finite value of vortex length (0.27 x upstream diameter) in the regime of creeping flow. Two additional kinematic characteristics may be defined for the vortex region:

(1) relative vortex intensity, defined as the ratio of the absolute value of maximum stream-function in the region of separated flow to the boundary value in the upstream developed flow and

(2) the ratio of the maximum absolute wall vorticity in the backflow region to the upstream boundary vorticity.

These two parameters increase in a similar manner with Reynolds number and appear to have asymptotic limits. Hence, although its length continues to increase linearly up to a Reynolds number of 200, the relative strength of the vortex does not appear to increase much beyond this limit.

1.3 Flow Regimes at Higher Reynolds Numbers

At higher Reynolds numbers a second flow regime has been observed (2), where shear layer waves and their stability play the dominant role. Its onset is marked by the attainment of a maximum value for reattachment length. Thereafter, reattachment is determined when the lateral extent of the undulating waves in the shear layer, which increase in amplitude as the Reynolds number is increased, spreads to the tube walls. Hence, within this flow region, the reattachment length decreases with increasing Reynolds number. In the turbulent region the reattachment length remains fairly constant at a value of about 10 step heights and is apparently not affected a great deal by either Reynolds number or tube diameter ratio (3).

1.4 Flow Development in the Laminar Regime

At the reattachment point the velocity gradient is zero. The velocity profile changes from bell-shaped just beyond this point to parabolic in the fully developed region with a corresponding decrease in centreline velocity. The flow is normally considered to be fully developed when the centreline velocity is within 1 % of the equilibrium value ($2\,V_{mean}$). The development length may be predicted from an experimentally determined velocity profile, which is used as the upstream boundary condition to the solution of the equations governing the flow of an incompressible fluid in a straight tube of axially unchanging cross-section.

2. THEORY

Three general analytical techniques have been developed for dealing with the problem of laminar flow in the entrance region of a tube of circular cross-section. Two of these (Atkinson - Goldstein (4) and Schiller (5)) require the formulation of equations which apply to the region of the developing boundary layer. The third method consists of linearizing the inertia terms in the axial Navier - Stokes equation and solving the resulting, much simplified equation of motion. It is this last method which appears to have greater flexibility and might be particularly useful in certain cases for predicting flow development when the upstream boundary condition is known, e.g. from experimental measurements.

This type of solution has been developed by Langhaar (6) and Targ (7), who applied it to the case of a circular section tube with uniform velocity at inlet. In subsequent paper by Sparrow et al. (8) a refinement of Langhaar's technique is presented solving the linearized axial momentum equation for the same condition at tube inlet, assuming radial momentum terms to be negligibly small. This assumption has been demonstrated to be quite reasonable (9) for the case of Reynolds numbers above about 100. For very small Reynolds numbers, the radial velocity component may be as high as 30% of the axial velocity component and therefore it is not really justifiable to neglect radial momentum terms in this case. However, the radial velocity component decreases fairly rapidly as one moves downstream from the tube entrance.

The axial Navier - Stokes equation for steady, axisymmetric flow may be written

$$v_r \frac{\partial v_z}{\partial r} + v_z \frac{\partial v_z}{\partial z} = g_z - \frac{\partial}{\partial z}\left(\frac{p}{\rho}\right) + \nu \left[\frac{1}{r} \frac{\partial}{\partial r}\left(r \frac{\partial v_z}{\partial r}\right)\right] \quad (2.1)$$

Two approximations which have been introduced into this equation are

(1) that the static pressure is a function of z alone and

(2) that the term $\partial^2 v_z/\partial z^2$ may be neglected. The latter is equivalent to the assumption that the derivative of the normal stress $\partial \sigma_{zz}/\partial z$ is the same as the pressure gradient.

Adopting for the present the notation of Langhaar (3), the terms on the left hand side may be approximated by $\nu\beta^2 v_z$, where β is a function of z only. This yields

$$\frac{Dv_z}{Dt} = v_r \frac{\partial v_z}{\partial r} + v_z \frac{\partial v_z}{\partial z} = \nu \beta^2 v_z \quad (2.2)$$

This equation is satisfied by $\beta = 0$ in the region of fully developed flow and is always satisfied at the tube walls, where v_z and v_r are both zero. For the inviscid core of a developing boundary layer model, equation (2.2) is satisfied by $\partial v_z/\partial z = \nu \beta^2$. The equation therefore applies exactly to regions where there is no radial momentum exchange taking place. Its application is not strictly valid within the devel-

oping boundary layer. However, it may be argued that linearisation based on equation (2.2) will allow a justifiable simplification to be made to the equations governing flow, provided that radial momentum exchange is always only a small proportion of axial convection, over most of the tube cross section.

Equation (2.1) may be written in the form

$$\beta^2 v_z = -\alpha + \frac{1}{r}\frac{\partial}{\partial r}\left(r\frac{\partial v_z}{\partial r}\right) \qquad (2.3)$$

where α and β are functions of z alone. Langhaar introduced the upstream boundary condition as the limit on an integral and obtained the solution to equation (2.3) in the form of a family of velocity profiles with parameter expressed as a function of the axial coordinate. This technique does not allow the introduction of a boundary condition which is a function of the independent variable.

Equation (2.1) may also be linearized by writing

$$\epsilon(z)\, V_m \frac{\partial v_z}{\partial z} = \Lambda(z) + \nu \nabla^2 v_z \qquad (2.4)$$

in which V_m is the mean velocity and ϵ and Λ are both functions of z. This obviously has the same form as equation (2.3) and no further justification for it is necessary. Its solution for an arbitrary upstream boundary condition is presented below.

Integrating equation (2.4) over the tube cross-section and noting that $\partial/\partial_z \int_A v_z \, dA = 0$ from continuity

$$\Lambda(z) = -\frac{2\nu}{R}\left(\frac{\partial v_z}{\partial r}\right)_{r=R} \tag{2.5}$$

and

$$\epsilon(z) V_m \frac{\partial v_z}{\partial z} = \nu\left[\frac{1}{r}\frac{\partial}{\partial r}\left(r\frac{\partial v_z}{\partial r}\right)\right] - \frac{2\nu}{R}\left(\frac{\partial v_z}{\partial r}\right)_{r=R} \tag{2.6}$$

A stretched coordinate, z^*, may be defined such that

$$dz = \epsilon(z)\, dz^* \tag{2.7}$$

Also, writing

$$v_z = (v_z)_{fd} + v_z^* \tag{2.8}$$

Equation (2.6) may be expressed in terms of the difference velocity, v_z^*, since it is a linear equation:

$$V_m \frac{\partial(v_z^*)}{\partial z^*} = \nu\left[\frac{1}{r}\frac{\partial}{\partial r}\left(r\frac{\partial v_z^*}{\partial r}\right)\right] - \frac{2\nu}{R}\left(\frac{\partial v_z^*}{\partial r}\right)_{r=R} \tag{2.9}$$

Introducing the following non-dimensional parameters

$$\eta = \frac{r}{R}, \quad Z = \frac{z/R}{V_m R/\nu}, \quad Z^* = \frac{z^*/R}{V_m R/\nu}, \quad \omega = \frac{v_z}{V_m}, \quad \omega^* = \frac{v_z^*}{V_m}$$

the above equation may be written

$$\frac{\partial \omega^*}{\partial Z^*} = \left[\frac{1}{\eta}\frac{\partial}{\partial \eta}\left(\eta\frac{\partial \omega^*}{\partial \eta}\right)\right] - 2\left(\frac{\partial \omega^*}{\partial \eta}\right)_{\eta = 1} \tag{2.10}$$

and is to be solved subject to the conditions

$$(1)\ \omega^* = 0 \quad \text{when} \quad \eta = 1 \quad \text{for all } Z^*$$

$$(11)\ \omega^* = f(\eta) \quad \text{when} \quad Z^* = 0$$

It is first necessary, however, to obtain a relationship between Z and Z^*. The following expression for ϵ may be derived by making use of the axial momentum equation and a mechanical energy equation derived from the former by multiplying throughout by v_z (Appendix 2):

$$\epsilon = \frac{\int_{\eta=0}^{\eta=1} (2\omega - 1.5\omega^2)\,\eta\,\frac{\partial \omega}{\partial Z^*}\,d\eta}{\left(\frac{\partial \omega}{\partial \eta}\right)_{\eta=1} + \int_{\eta=0}^{\eta=1} \eta \left(\frac{\partial \omega}{\partial \eta}\right)^2 d\eta} \qquad (2.11)$$

With ω a known function of η and Z^*, the right hand side of equation (2.11) can be evaluated. Hence ϵ may be determined as a function of Z^* and the relationship between Z and Z^* is given by

$$Z = \int_0^{Z^*} \epsilon \; dZ^* \qquad (2.12)$$

The solution of equation (2.10) has the form

$$\omega^* = \sum_{i=1}^{\infty} c_i \; g_i(\eta) \; e^{-\alpha_i^2 Z^*} \qquad (2.13)$$

where

$$g_i(\eta) = \frac{2}{\alpha_i} \left\{ \frac{J_o(\alpha_i \eta) - J_o(\alpha_i)}{J_o(\alpha_i)} \right\} \qquad (2.14)$$

and the α_i are the roots of the equation

$$J_1(\alpha_i) / J_o(\alpha_i) = 0.5\,\alpha_i \qquad (2.15)$$

The coefficients c_i are obtained by making use of the upstream boundary condition. If the non-dimensional axial velocity, ω, is expressed as a polynomial in η of degree (N-1), i. e.

$$\omega = f(\eta) = B(1) + B(2)\eta + B(3)\eta^2 + \text{---} + B(N)\eta^{N-1} \qquad (2.16)$$

then it may be shown that

$$c_i = \frac{2}{\alpha_i} - \frac{4}{\alpha_i}\left\{\frac{B(1)}{2} + \frac{B(2)}{3} + \frac{B(3)}{4} + \text{---} + \frac{B(N)}{N+1}\right\}$$

$$+ \frac{4}{\alpha_i J_o(\alpha_i)}\left\{\frac{B(1)(\phi_1)}{\alpha_i^2} + \frac{B(2)(\phi_2)}{\alpha_i^3} + \text{----} + \frac{B(N)(\phi_N)}{\alpha_i^{(N+1)}}\right\} \qquad (2.17)$$

where

$$\phi_N = \int_0^{\alpha_i} \chi^N J_o(\chi)\, d\chi$$

A detailed explanation of the procedure for obtaining the solution is presented in Appendix 2.

3. DESCRIPTION OF APPARATUS

3.1 Flow System

A schematic diagram of the flow system is presented in Figure 1. The essential components of the system were as follows:

(1) Fluid Suspension

(2) Model of Circular Tube with Abrupt Expansion

(3) Mixing Chamber

(4) Motor/Pump Unit

(5) Pulsation Damper

(6) Venturimeter

3.1.1 The Fluid Suspension

The composition and properties of the suspending medium are detailed in Table 1. The graph of Figure 2 shows its viscosity - temperature characteristic over the temperature range encountered during the experiments. This data was obtained with the aid of a cone and plate viscometer (Wells - Brookfield Micro Viscometer) which allowed viscosity to be measured at constant shear rate. It was possible to affirm that the fluid was Newtonian in behaviour, since the shear rate could be varied by changing the cone angle and/or the speed or rotation of the cone and since, for a Newtonian fluid, shear stress (and hence the restraining torque on the cone) is directly proportional to shear rate. The refractive index of the solution was matched to that of a 95% by weight glycerol, aqueous glycerol solution (section 3.2.1), and the specific gravity was adjusted, by addition of n-amyl alcohol, to that of the polystyrene particles which constituted the suspended phase (1.04). The suspension contained particles of up to 420 μ diameter, the majority of which had been selected from a batch of between 150μ and 300μ.

DESCRIPTION OF SYMBOLS USED IN FIGURE I

A	Mixing Chamber
B	Teflon Expansion Piece
C	Viewing Cell
D	Optical Table
E	Mercury Manometer
F	Motor
G	Pump
H	Speed Control
I	Venturimeter
J	Double U-Tube Manometer
K	QVF Thick Wall Glass Tubing

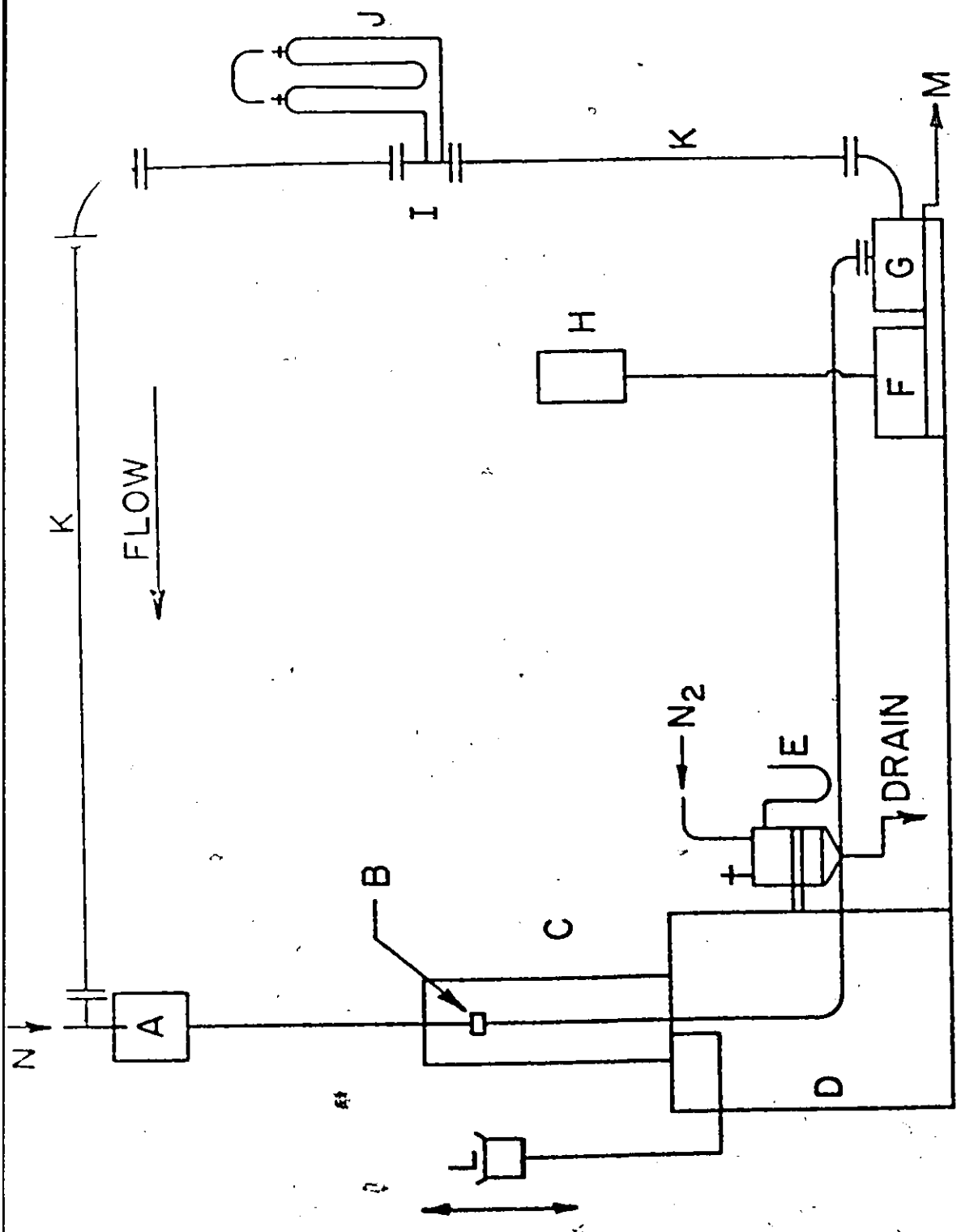

FIGURE 1 SCHEMATIC DIAGRAM OF FLOW SYSTEM

PROPERTIES OF COMPONENTS (corresponding to a temperature of 20°C)			
	BENZYL ALCOHOL	ETHYLENE GLYCOL	n-AMYL ALCOHOL
SPECIFIC GRAVITY	1.045	1.111	0.817
REFRACTIVE INDEX	1.5396	1.4318	1.4101
NORMAL BOILING POINT	204	198	137.75

PERCENTAGE COMPOSITION BY VOLUME		
BENZYL ALCOHOL	AQUEOUS ETHYLENE GLYCOL (50% ETHYLENE GLYCOL)	n-AMYL ALCOHOL
58	38	4

PROPERTIES OF SUSPENDING FLUID (measured at 20°C)		
REFRACTIVE INDEX	SPECIFIC GRAVITY	VISCOSITY
1.466	1.04	Given in Figure 2

TABLE I COMPOSITION AND PROPERTIES OF SUSPENDING FLUID

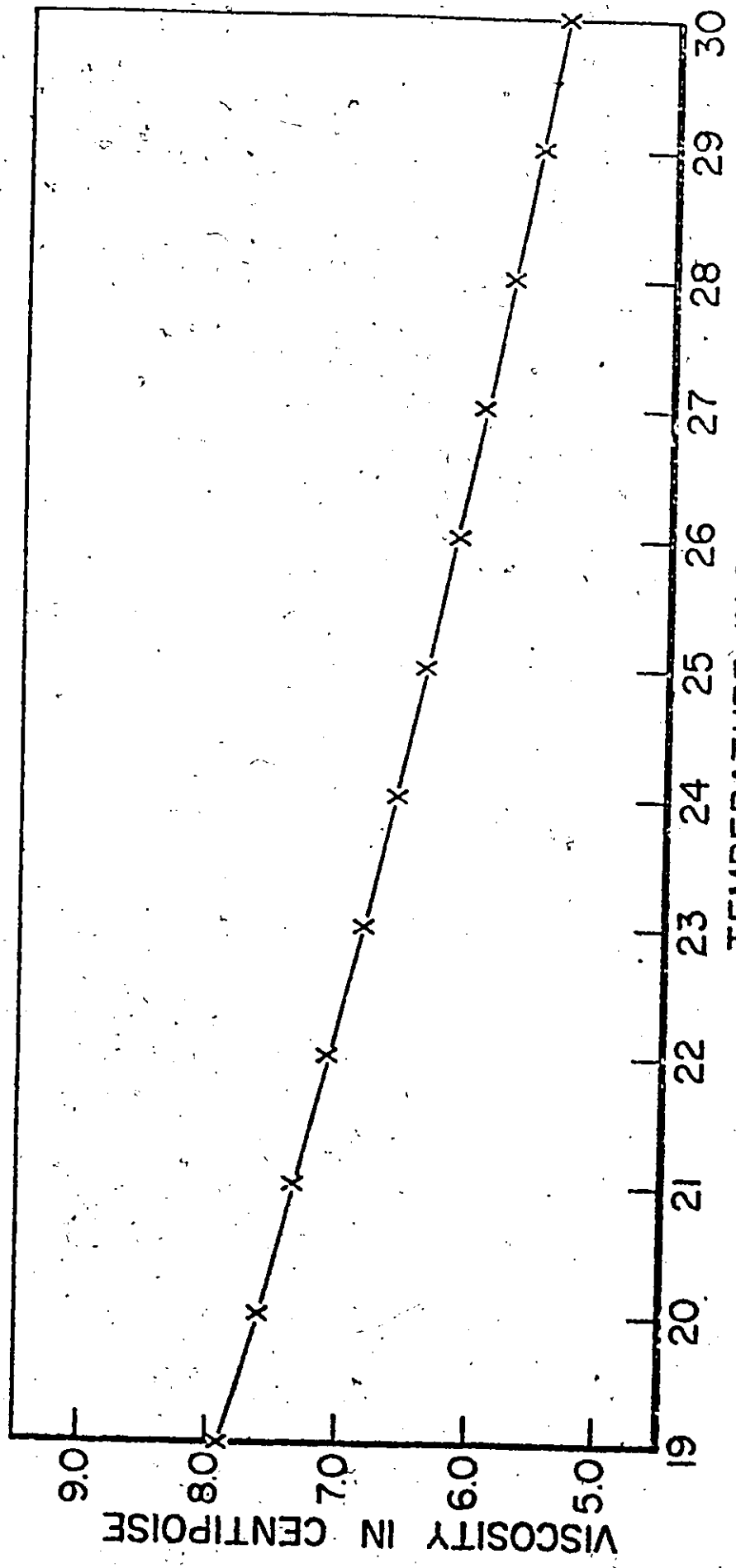

FIGURE 2 - VISCOSITY - TEMPERATURE CURVE FOR SUSPENDING FLUID

Observation of a sample of the suspension over a period of several days, through a temperature range of 20 - 25°c, led to the conclusion that the density difference between the two phases was so small that sedimentation rates might be considered negligible. The concentration was adjusted to about 5 particles/cc (except for direct visual observation of the vortex, where the concentration was considerably changed).

3.1.2 Model of Circular Tube with Abrupt Expansion

The vertical limb on the left hand side of figure 1 constituted the model. It consisted of two lengths of glass tube connected by a teflon transition piece (figure 3) with viton "O" rings on the inside periphery to ensure effective sealing, the total length of the limb being 90". The length of the upper tube was sufficient to allow the development of a Poiseuillean velocity distribution just upstream of the expansion at the highest flow rate required (chapter 4). This tube was interchangeable with three others, each of different diameter (table 2), providing step-diameter ratios, d/D, of 0.63, 0.79, 0.93 and 1.00. These values were obtained from the tube internal diameters, measured with the aid of vernier calipers at the expansion end of each tube, as indicated in Figure 3.

3.1.3 The Mixing Chamber

Figure 4 shows the mixing chamber, which was an aluminium cylinder with provision at the base for a concentrically located aluminium insert attached to the top of each of the smaller diameter glass tubes. The internal profile of each of the four inserts was machined to blend with the

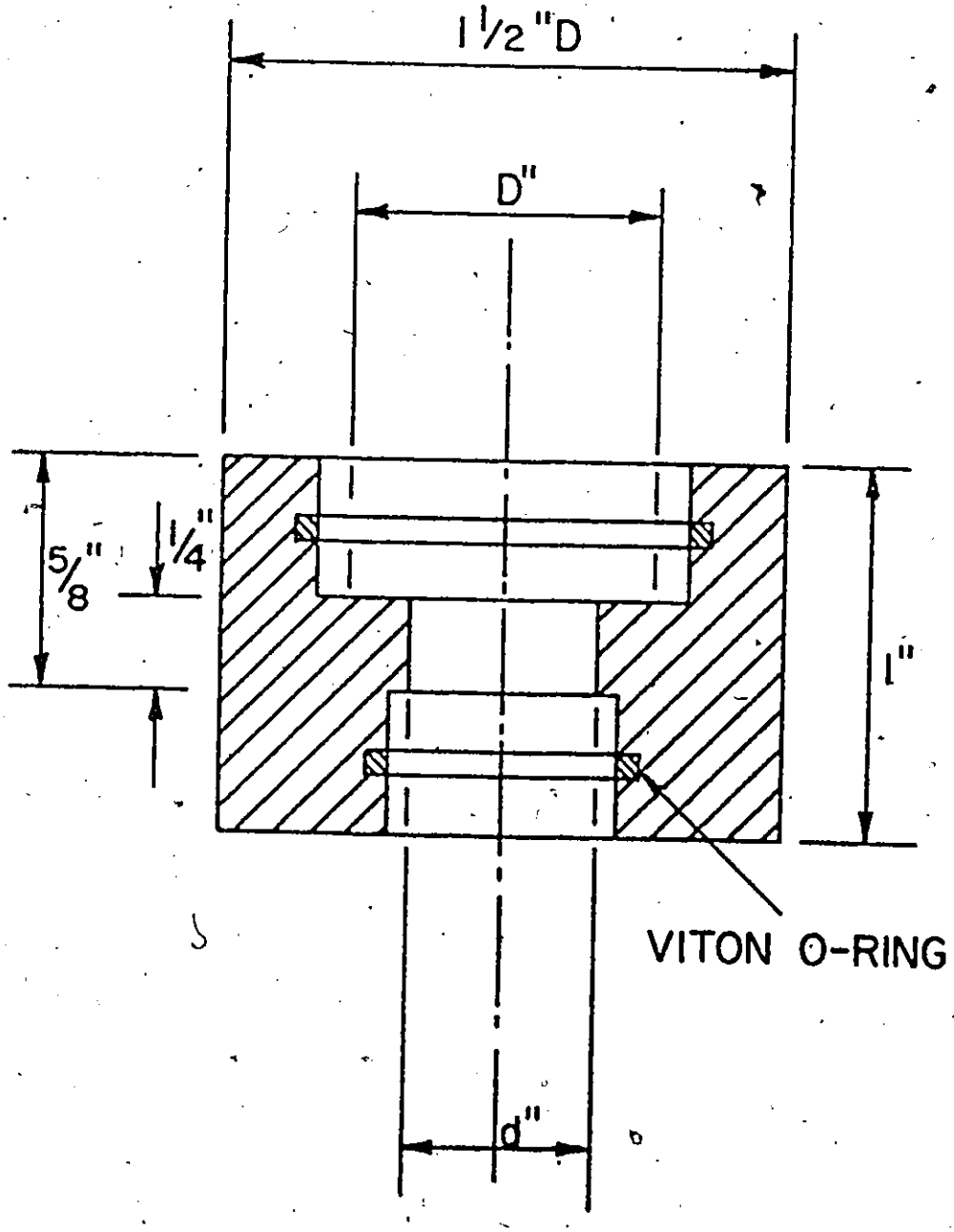

FIGURE 3 TEFLON EXPANSION PIECE

MEAN DIAMETER OF SMALLER TUBE AT STEP (d cm.)	1.298	1.627	1.916	2.06
MEAN DIAMETER OF LARGER TUBE AT STEP (D cm.)	2.06	2.06	2.06	2.06
DIAMETER RATIO (d/D)	0.63	0.79	0.93	1.0

LENGTH OF UPPER TUBE = 47 INCHES (119 cm.)
LENGTH OF LOWER TUBE = 43 INCHES (109 cm.)

TABLE 2: DIMENSIONS OF GLASS TUBES

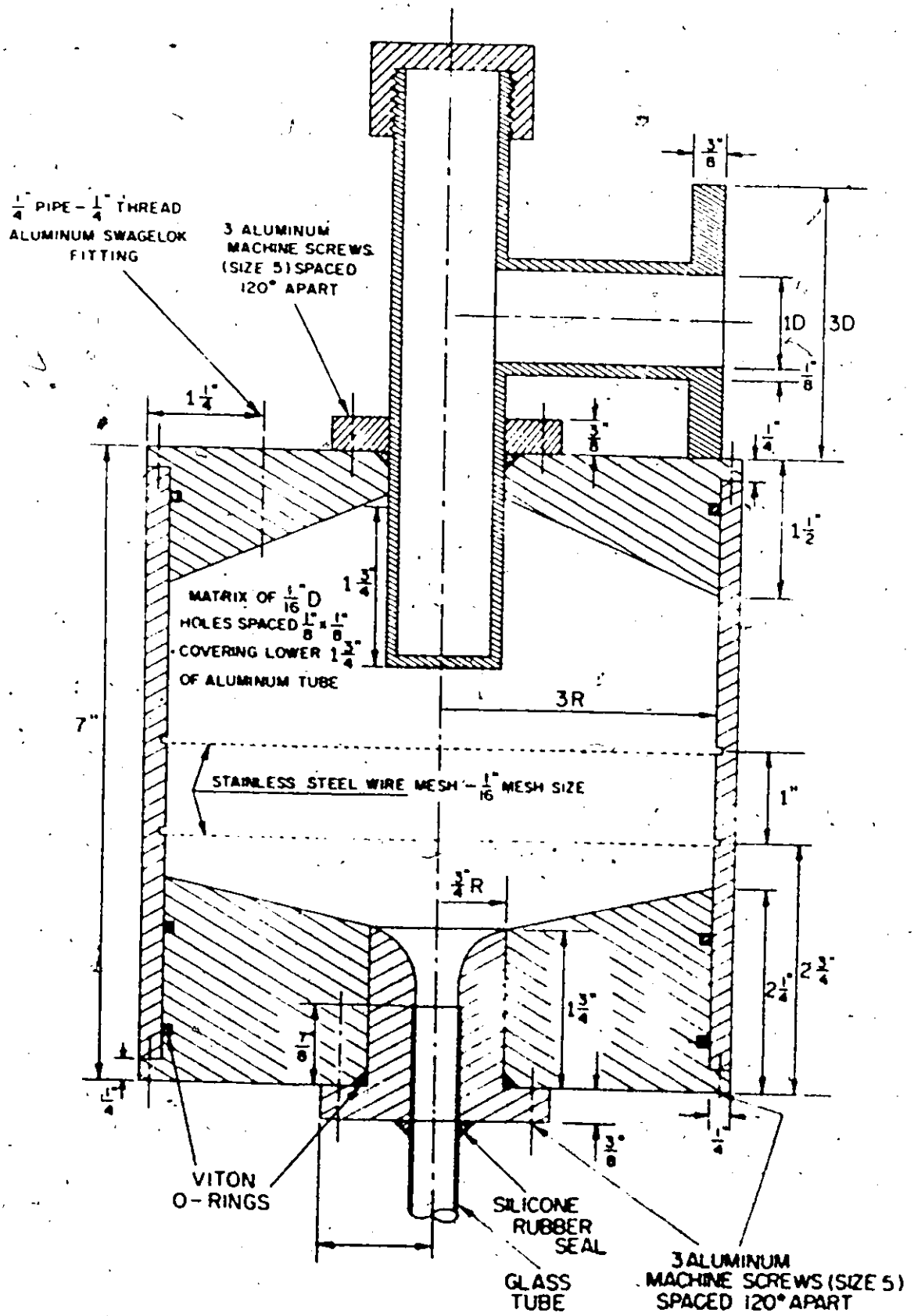

FIGURE 4 - MIXING CHAMBER

sloping base of the chamber.

Homogeneous mixing of the suspension was ensured by forcing it to pass through a matrix of 1/16" diameter holes drilled into the lower two inches of the aluminium tube. Any small-scale turbulence thus generated was removed by the presence of a double layer of wire mesh. In order to facilitate the expulsion of air from the system when charging with the fluid suspension, the inside top of the chamber was machined to slope upwards from the walls. A 0.2°C thermometer was provided at the top of the chamber for recording the temperature of the fluid prior to its entry into the upper glass tube.

3.1.4 Motor/Pump Unit

The pump used was a Moyno type SSF pump driven by a 1/2 h.p., d. c. motor with a 110 volt SCR speed control. This pump, which is of the positive displacement type, is particularly suitable for handling solid/liquid suspensions and provides a fairly uniform flow. The stator and rotor were of viton and stainless steel construction respectively so that no problems were encountered with pump corrosion or contamination of fluid.

A pulsation damper was incorporated into the system in order to remove the small pressure fluctuations produced by the pump. It consisted of an inverted glass bottle with three tappings at the top, one of which was connected to a mercury manometer and another to the pressure regulator of a nitrogen cylinder. The third was a bleed to atmosphere. The

purpose of this arrangement was to keep the pressure in the bottle constant as the flow rate was changed. However, as the pressure variation was found to be quite small over the experimental range of flow rates, this was considered unnecessary and the function of the device was solely as a damping system.

3.1.6 Venturimeter (Figure 5)

The venturimeter was made of aluminium with two piezometer openings set 1-1/4 inches apart. It operated in conjunction with a double U-tube manometer which had two air columns of equal length separating the manometric fluid (water) from the circulating fluid. The two air columns could be bled together to level the liquid surfaces before the commencement of an experiment. The characteristic curve for this flowmeter is given in Figure 6.

3.2 Optical Equipment

(1) Viewing Cell

(2) Optical Table

(3) High Speed Camera

(4) Camera Regulator

(5) Timing Light Generator

(6) Arc Lamps and Plano - Convex Lenses

(7) Photo-Optical Data Analyser

3.2.1 Viewing Cell (Plate 1)

The region of the flowfield that was of experimental interest extended from a few diameters upstream of the expansion to about 20 diam-

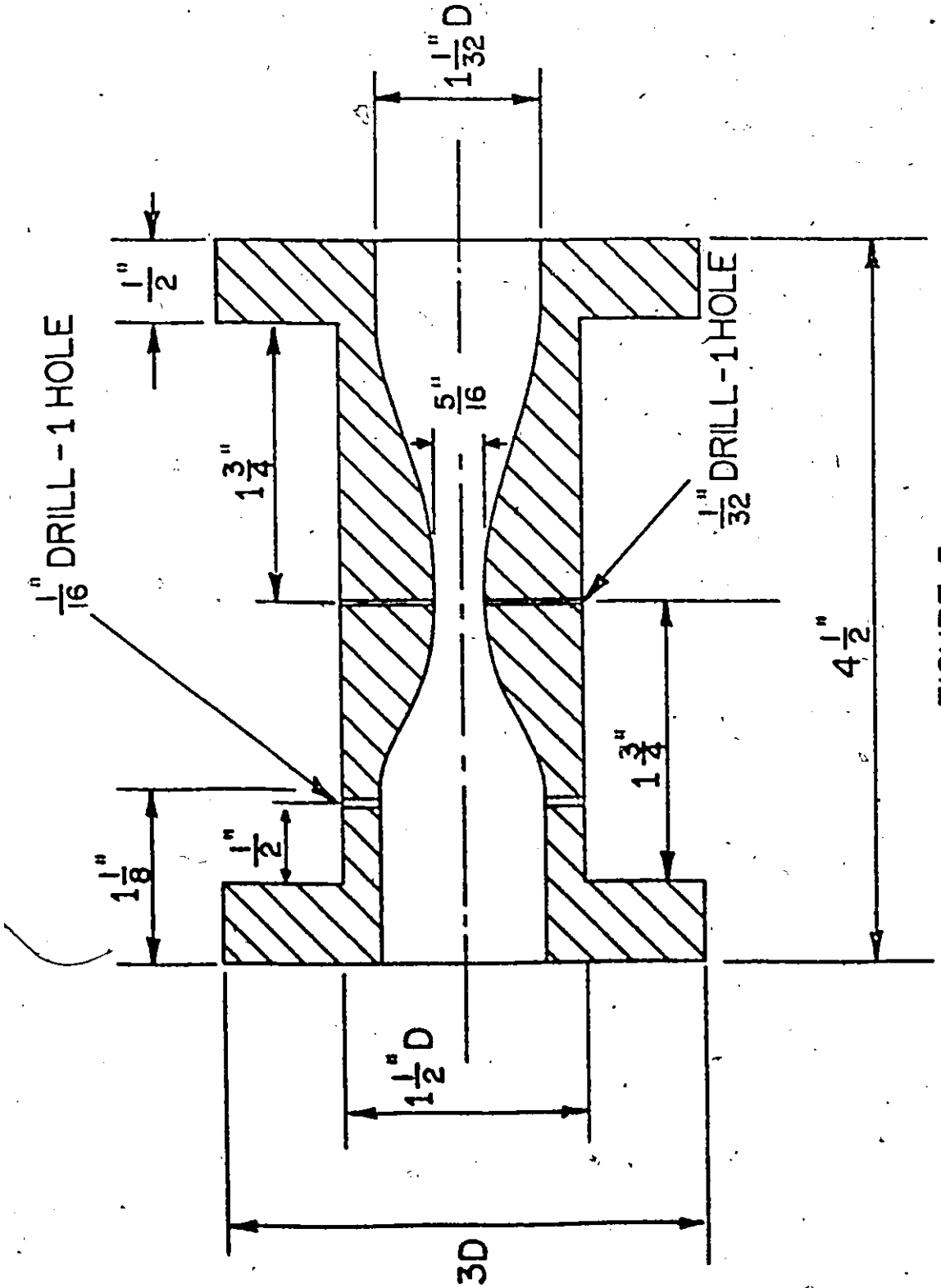

FIGURE. 5 - ALUMINIUM VENTURIMETER

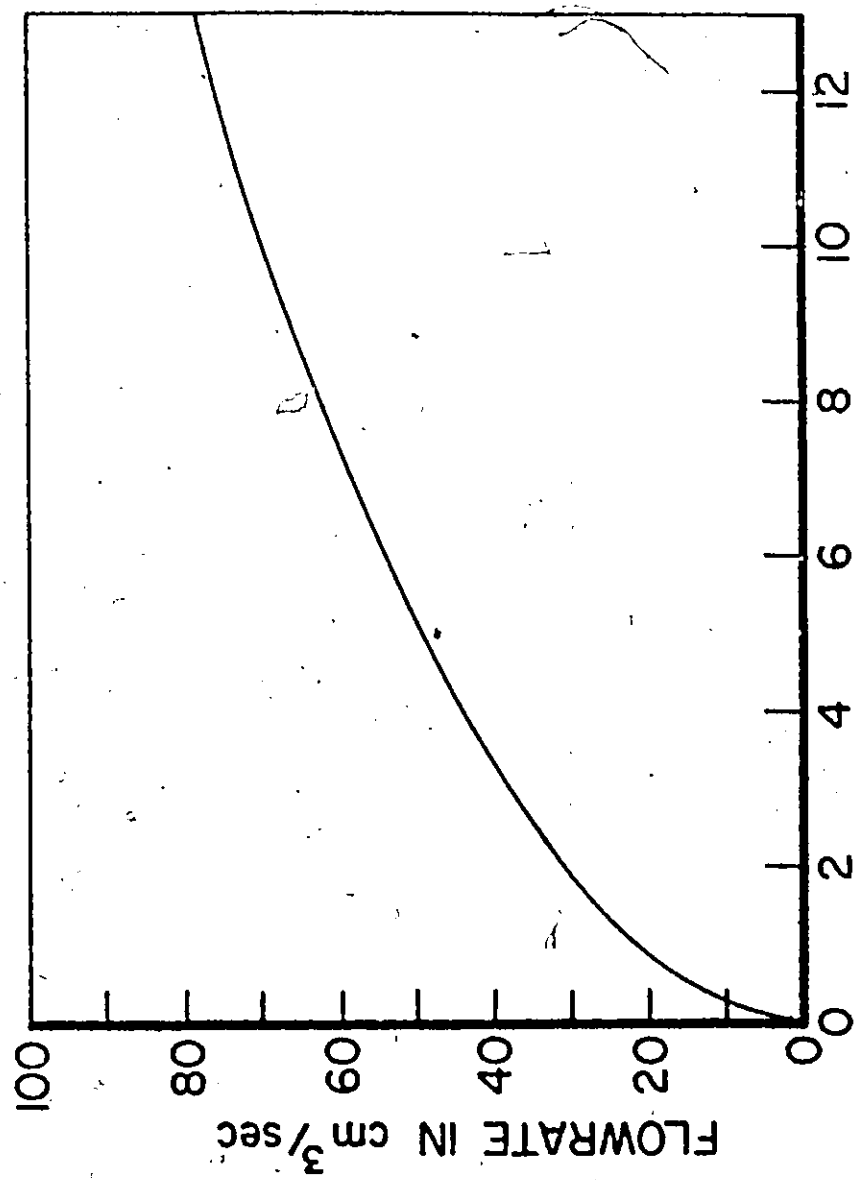

FIGURE 6 VENTURIMETER CALIBRATION CURVE

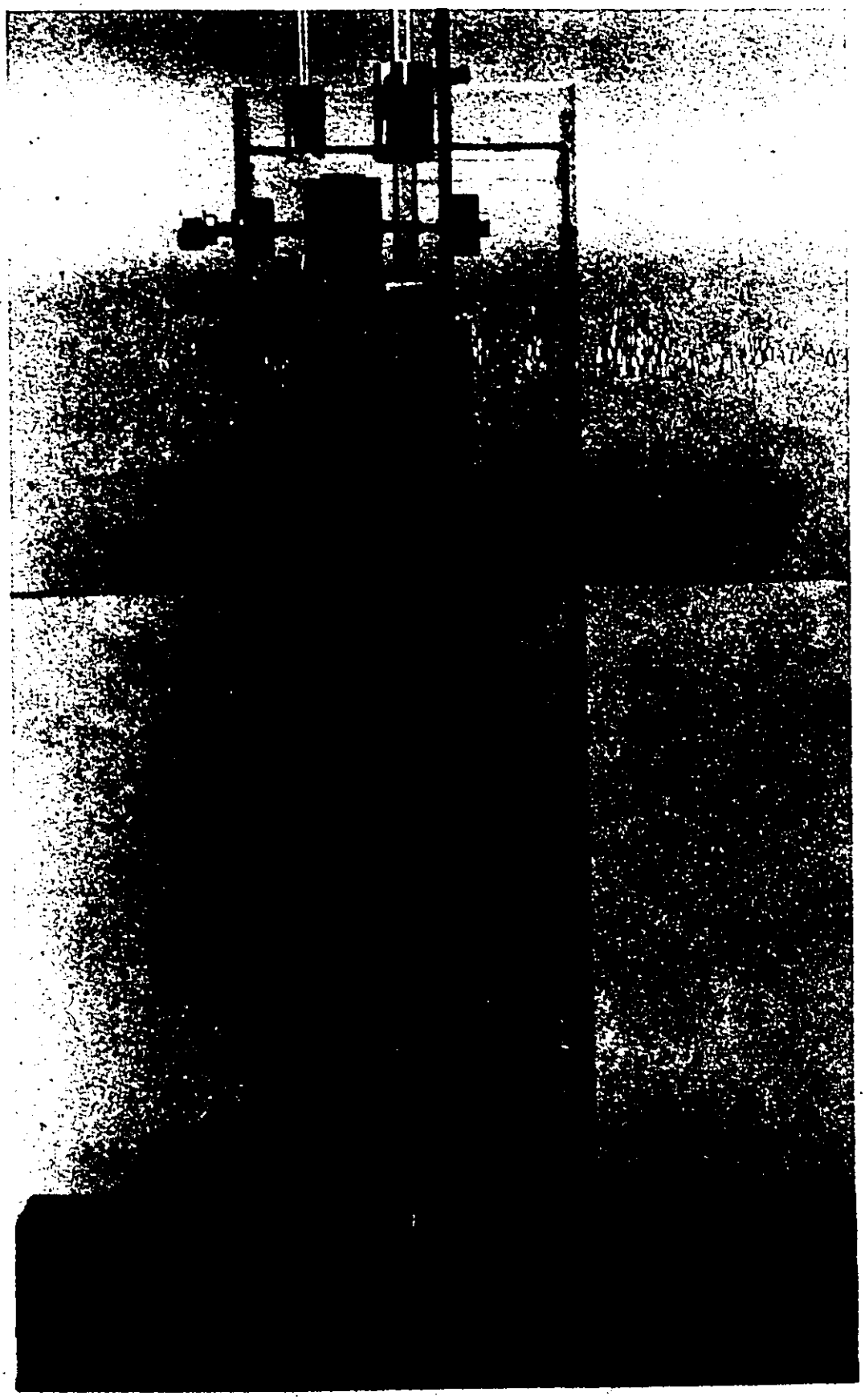

PLATE 1 - VIEWING CELL

eters downstream. This section of the model was enclosed in a rectangular perspex cell, 30-1/2" x 9" x 2-7/8", which was secured to the top of a steel table. Inside the cell were two front surface reflecting mirrors, 2-1/2" x 3/4", each set in a brass mount with its surface inclined at an angle of 45^{o} to the base of the mount and positioned so as to provide a two dimensional view of one of the upper quadrants of the glass tube (Plate 2).

The mirror placed above the teflon expansion piece was constrained to move horizontally. Its purpose was to allow a section of the tube upstream of the expansion to be filmed to determine whether the upstream boundary condition was satisfied at the highest Reynolds number (i.e. to determine whether the velocity profile there was parabolic). When the upper tube was replaced with one of smaller diameter, the mirror was moved to the right to bring its edge in contact with the tube wall.

The brass mount containing the second mirror moved vertically in an aluminium track, its position adjusted by means of a steel rod passing through the mount and through the top of the cell and retained there by a steel collar. The flow pattern could thus be recorded photographically at any axial location throughout the region of interest.

To facilitate changing the upper glass tube, the face of the cell was removable, with sealing provided by a 1/16" diameter rubber cord set in a groove machined around the perimeter of the cell. The cell was filled from the bottom with an aqueous glycerol solution. By matching the refractive index of the glycerol to that of the fluid inside the tube (1.466),

PLATE 2 - FRONT SURFACE REFLECTING MIRROR IN BRASS MOUNT

optical distortion due to refraction of light was reduced considerably. Since the glycerol was diluted with 5% water, its viscosity was reduced by about half, thus making it much easier to fill the cell. The maximum error incorporated by not having the refractive index of the glycerol and circulating fluid matched exactly to that of glass (1.474) was estimated as 1 % of the tube diameter (Appendix 4). This error appears in the form of a linear displacement of the image of the particle centre.

3.2.2 Optical Table

A table was constructed to provide a rigid support for both the viewing cell and the high speed camera. It consisted of a frame 30" x 24" x 36" high, fabricated from steel angle with levelling screws at the base and a 10" wide aluminium plate fitted to the top. The camera was carried by a one-inch diameter brass rod which could slide vertically in a sleeve attached to the aluminium plate. Slots milled into the plate enabled the sleeve to be moved toward or away from the cell, allowing the camera freedom of motion both vertically and horizontally.

The viewing cell was positioned eccentrically with one side aligned with the edge of the aluminium plate. This arrangement meant that with the axis of the camera lens at right angles to the face of the cell, the outer wall of the larger diameter glass tube would be located at the exact centre of the field of view.

3.2.3 High Speed Camera (Plate 3)

Photographic data was obtained with the aid of a Hycam cine camera

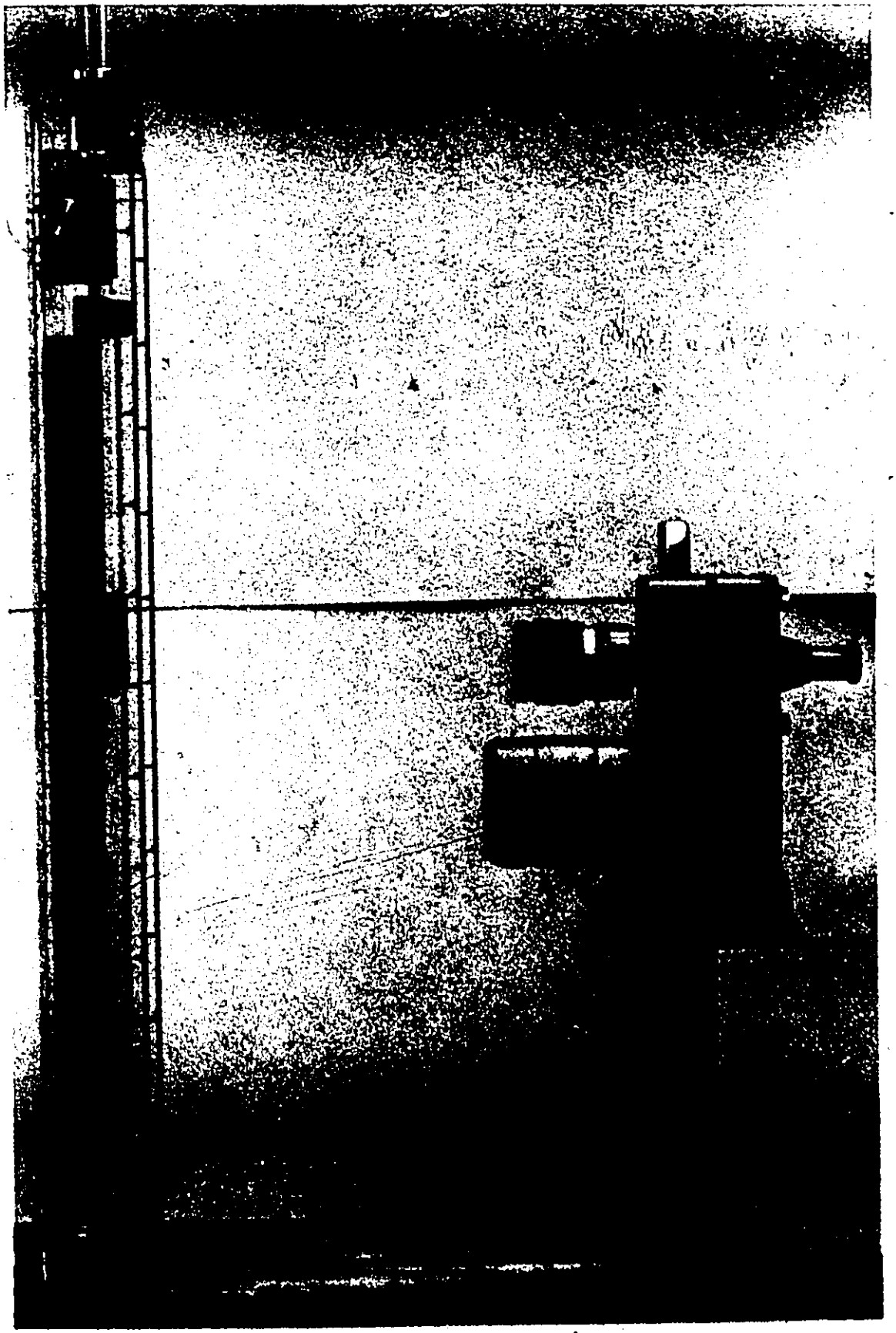

PLATE 3 - SIDE VIEW OF HIGH SPEED MOVIE CAMERA & VIEWING CELL

(model K2001R). This was a 16 mm. high speed camera utilizing a rotating prism for optical compensation. With the aid of an electronic speed control unit, it was possible to vary the frame rate from 10 to 3,000 full frames per second. A 55 mm. f 2 Asahi Pentax lens was used, together with a small extension tube, to provide an image of an area approximately one inch square, the depth of field being about 1/2 inch.

The film used was Eastman Kodak Double-X Negative 7222 and Eastman Kodak Plus-X Negative 7231 on 100 foot reels, the latter being a material of finer grain. Both types produce a negative image when processed and for this particular application there appeared to be very little to choose between them.

3.2.4 Camera Regulator

The chart of figure 7 gives the speed curves throughout the regulated range. These curves were used to determine the exposure time for a given frame rate as outlined in Chapter 4.

3.2.5 Timing Light Generator

A reasonably accurate estimate of frame rate was obtained with the aid of a Milli-Mite TL9-4 timing light generator. This resulted in a series of pulses, 30 microseconds in width, appearing on the side of the film at a selected frequency of either 10 or 100 pulses/second, to within $\pm$ 1%.

3.2.6 Illumination

A strong point source of light was provided by a 100 watt carbon lamp which was placed at the focal point of a 6 inch focal length, plano-convex lens to produce a parallel beam 2 inches in diameter. The object

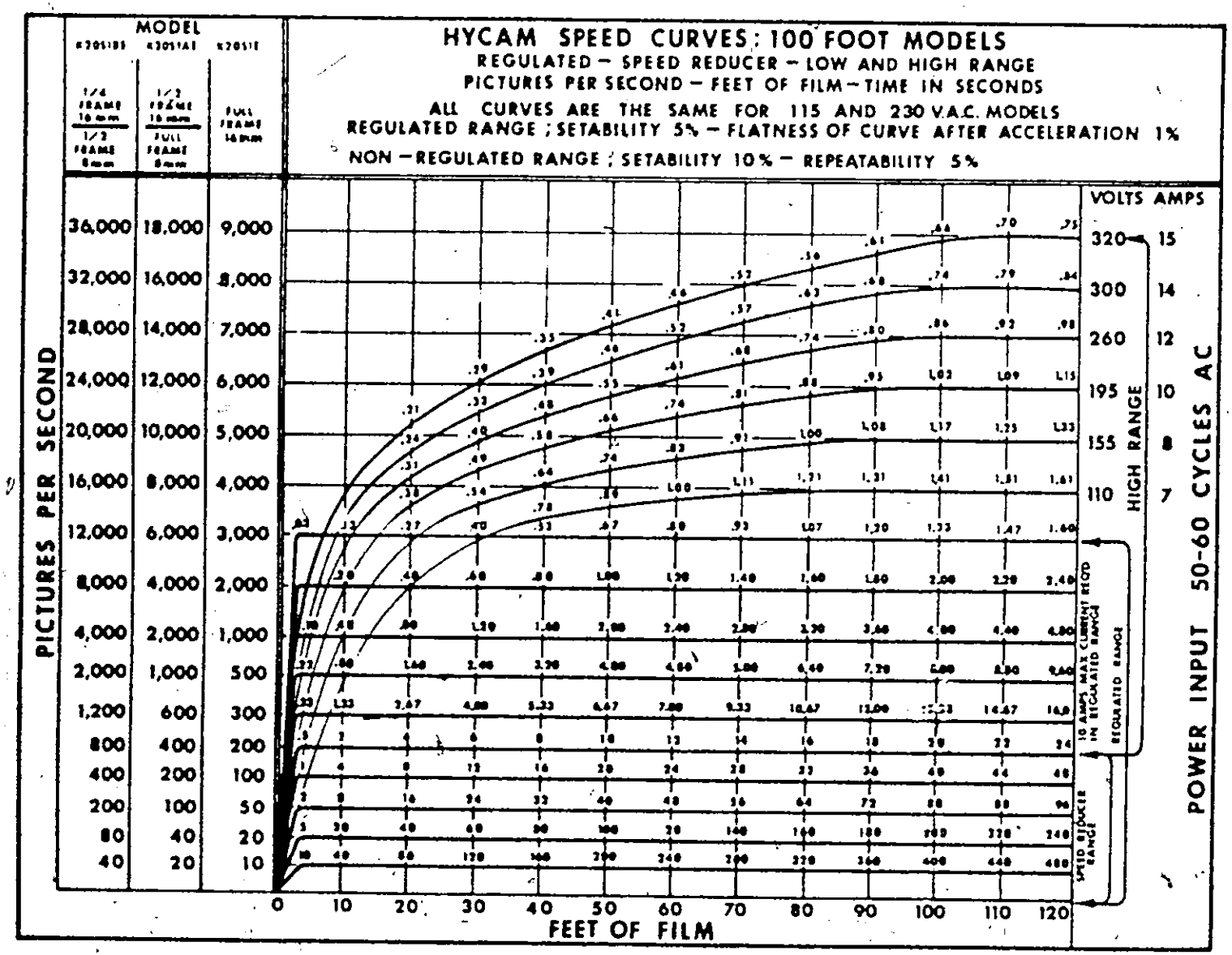
HYCAM SPEED CURVES: 100 FOOT MODELS
REGULATED – SPEED REDUCER – LOW AND HIGH RANGE
PICTURES PER SECOND – FEET OF FILM – TIME IN SECONDS
ALL CURVES ARE THE SAME FOR 115 AND 230 V.A.C. MODELS
REGULATED RANGE ; SETABILITY 5% – FLATNESS OF CURVE AFTER ACCELERATION 1%
NON – REGULATED RANGE ; SETABILITY 10% – REPEATABILITY 5%
MODEL
1/4 FRAME 16 mm / 1/2 FRAME 8mm
1/2 FRAME 16 mm / FULL FRAME 8mm
FULL FRAME 16mm
PICTURES PER SECOND
36,000 18,000 9,000
32,000 16,000 8,000
28,000 14,000 7,000
24,000 12,000 6,000
20,000 10,000 5,000
16,000 8,000 4,000
12,000 6,000 3,000
8,000 4,000 2,000
4,000 2,000 1,000
2,000 1,000 500
1,200 600 300
800 400 200
400 200 100
200 100 50
80 40 20
40 20 10
0 10 20 30 40 50 60 70 80 90 100 110 120
FEET OF FILM
VOLTS AMPS
320 15
300 14
260 12
195 10
155 8
110 7
HIGH RANGE
10 AMPS MAX CURRENT REQD IN REGULATED RANGE
REGULATED RANGE
SPEED REDUCER RANGE
POWER INPUT 50-60 CYCLES AC

FIGURE 7

was illuminated by two such beams, one from the side and one from the rear, intersecting at right angles. It was necessary to reduce the light intensity at most filming speeds in order to avoid over-exposure, and this was accomplished by placing a shade plate in front of the camera lens at right angles to its axis.

3.2.7 Photo - Optical Data Analyser

Film analysis was carried out with the aid of an L - W Photo Inc., Photo - Optical Data Analyser (model 224 - A), which was set up in a specially constructed rig to allow back-projection on to a transparent screen. The frame rate could be set, from a remote hand-held unit, to any of several different settings between 2 and 24 f.p.s., or the film could be projected frame by frame.

4. EXPERIMENTAL PROCEDURE

In setting up the apparatus, great care was taken to ensure that the left hand limb was as near vertical as possible and, more important, that the two tubes were coaxial. A plumbline was used for this purpose and lay along the axis of the tubes when viewed from two mutually perpendicular directions. Observation of the vortex led to the conclusion that there was very little asymmetry present in the flow.

The aluminium track had horizontal lines scribed at intervals of 1/2 inch along the length of the land adjacent to the tube wall. With the camera in its lowest position, the marking located at a distance of 14.875 inches from the step appeared in the centre of the field of view. When the camera was raised to a new position, usually through a distance of three or five inches, a short exposure was made with the track illuminated from the front. Hence a horizontal line appearing on the first film sequence provided the axial location for the determination of the velocity profile. The magnification factor was obtained from the width of the land, which had been accurately machined to 1/4 inch. The internal diameter of the larger tube was also determined photographically, with the camera displaced 1/2 inch to the left. The tube was found to be of uniform diameter over the first 18 inches of its length.

In order to obtain sufficient accuracy in measuring particle velocities, the frame rate was set to a value of at least $40\ q\ /\ \pi\ d^2$, q being the flow rate and d the diameter of the smaller tube. This meant that the

motion of the fastest moving particle (assuming it to move with the upstream fully developed centre line velocity) would be recorded on at least 10 frames as it moved across the field of view, which was approximately 2 cm. in height. The time required to expose a 25 ft. length of film (1000 frames) was then obtained from the curves of figure 7. The timing light generator was set to give at least one pulse per 30 frames.

With the camera in its lowest position the object was brought into focus in the normal way. The arc lamps and plano-convex lenses were carefully aligned to produce two mutually perpendicular, intersecting beams. The flowrate was adjusted to the desired value and the fluid suspension circulated for a while to allow it to become homogeneous. Its temperature was then recorded. A film was loaded into the camera and the first 25 feet exposed (this included a view of the aluminium track, taken under normal lighting conditions). The camera was then raised to its next position and a check was made, by looking through the eyepiece at the image on the film, to ensure that the outer wall of the glass tube was located at the centre of the field of view. Another 20 to 25 feet of film was exposed. The temperature was again recorded and the flowrate increased to a new value. It was then necessary to make a new frame rate setting in the manner outlined above. The remainder of the film was used up, with the camera finally back in its original position, the objective lens level with the 14.875 inch mark on the aluminium track. In this way, five film sequences were usually obtained for each experiment. Lastly, one more temperature reading was made.

Figure 8 illustrates the way in which quantitative data was obtained from the cine films. The inner wall of the tube appeared clearly in each view and the centreline was constructed by taking the distance R to be one half of the photographically determined diameter at axial location Z. Hence, non-dimensional particle coordinates η_x and η_y were determined by direct measurement. Particle velocities were obtained at, or very close to the horizontal line drawn at Z by allowing the particle to move through a distance of 1 to 1-1/2 cm. either side of the line and determining the corresponding time increment, $2\Delta t$, from the camera frame rate. Each velocity profile was constructed from 20 to 30 such velocity measurements.

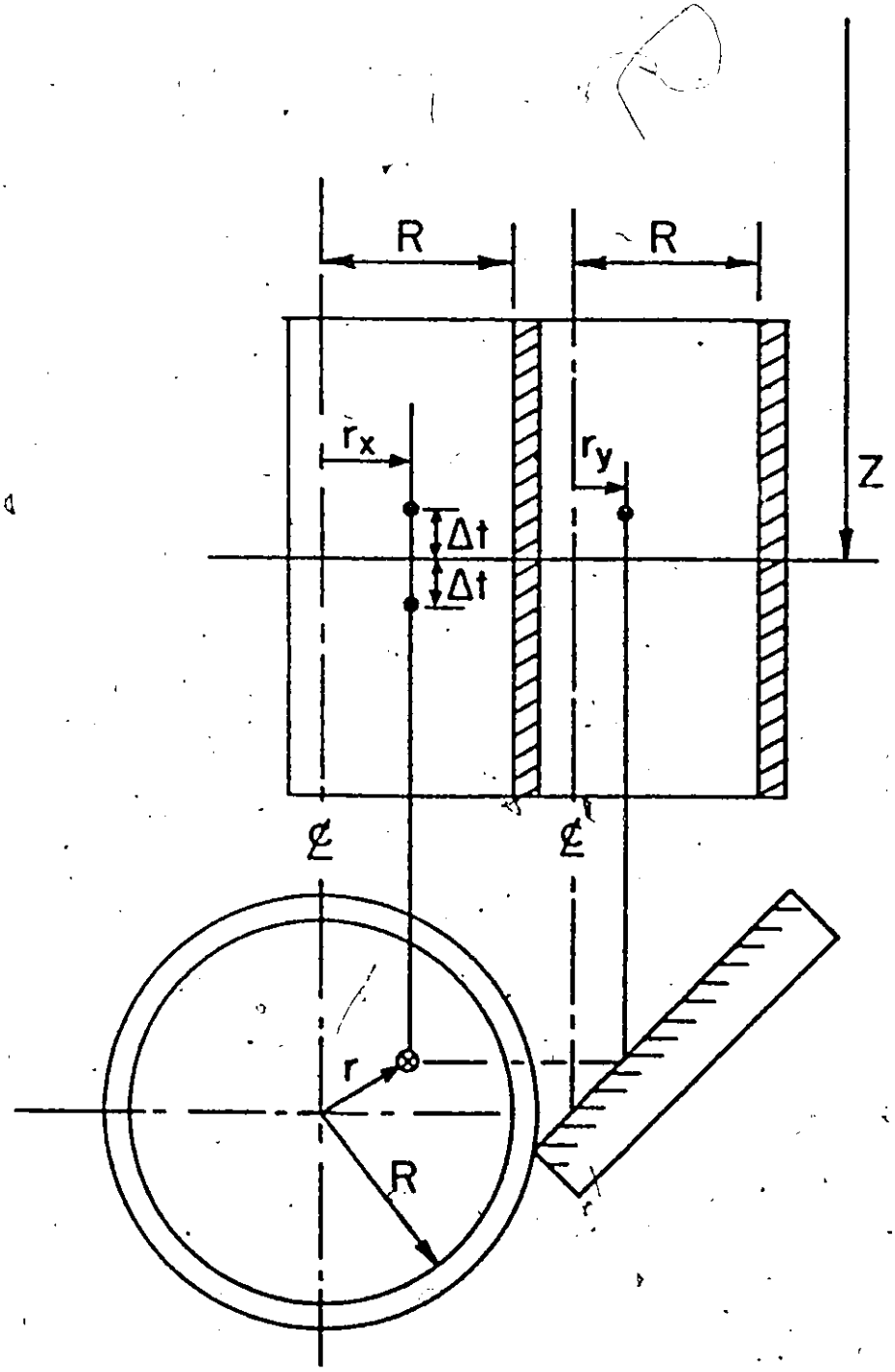

FIGURE 8 FILM ANALYSIS

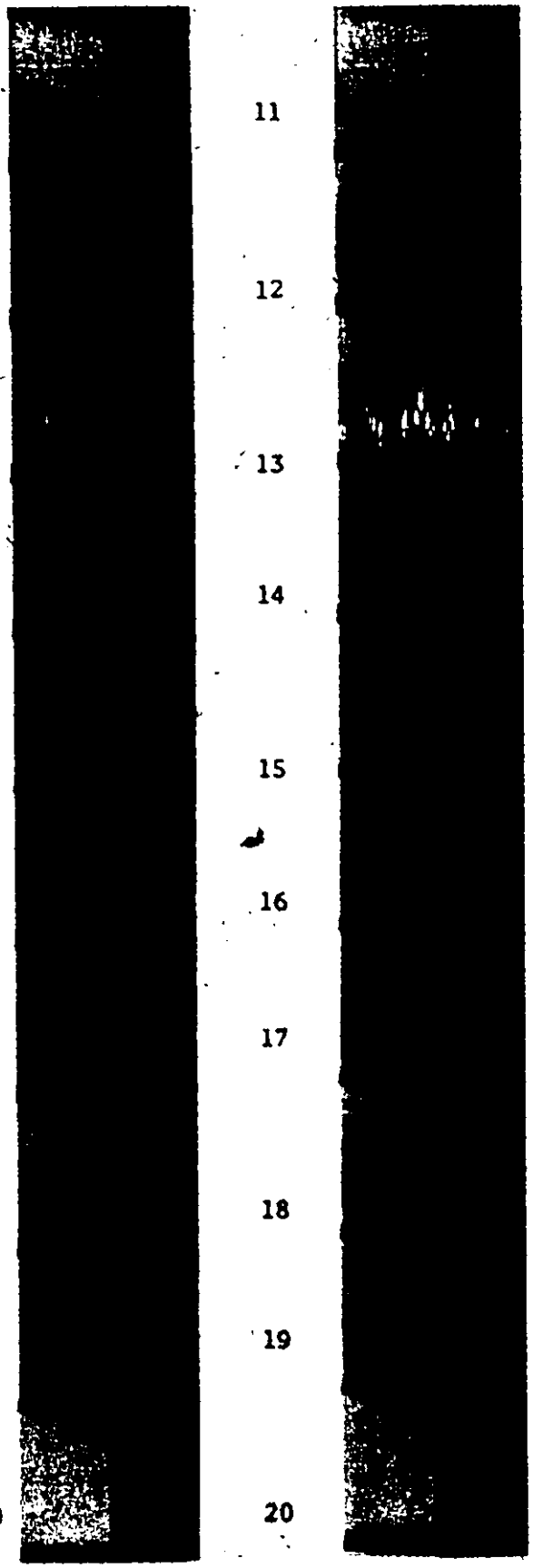

PLATE 4 - SEQUENCE OF 20 FRAMES FROM 16mm. FILM
THIS IS A POSITIVE (REVERSED) IMAGE

5. RESULTS AND DISCUSSION

5.1 Flow Development

Experimental and computational results are presented in the following tables and charts. Figure 9 illustrates the scheme whereby each velocity profile is denoted by two characters and a single subscript. The subscripts 1 and 2 refer to the upstream and downstream stations respectively, these being exactly 12.7 cm apart, with station 1 located 25 cm. from the step.

No mathematical representation is provided for the velocity profiles in one case ($d/D = 0.63$, $Q = 53.94$) because very little experimental data was obtained in the central region of the tube at station 2, where it was found that the velocity gradient at the wall was close to zero. Hence, for this particular case, the reattachment length was approximately 38 cm. and station 1 was situated inside the vortex region.

The experimental data listed in appendix 7 and plotted in figures 10 to 17 was obtained by measuring the velocities of the smaller particles in the flow. However, velocity measurements taken from particles with diameters of at least twice those of the smaller particles are included in figure 11 for comparison. The particle/fluid slip velocity has been shown (Appendix 1) to be inertial in origin; i.e. it is dependent upon particle size and velocity. The functional relationship is given in the appendix in terms of tube Reynolds number and particle to tube diameter ratio. However, although the experiment to which figure 14 refers was not carried out at the highest tube Reynolds number, particle velocities

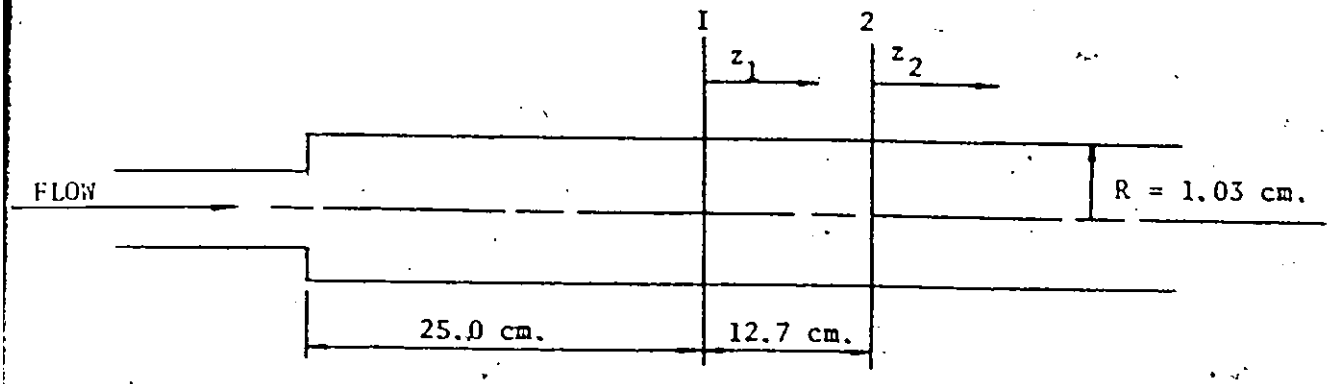

d/D / Q	0.63	0.79	0.93	
22.02	X	X	X	1
38.14	X	X	X	2
53.94		X	X	3
	A	B	C	

FIGURE 9 -EXPERIMENTAL NOTATION - X INDICATES THAT DATA HAS BEEN OBTAINED FOR THIS EXPERIMENT

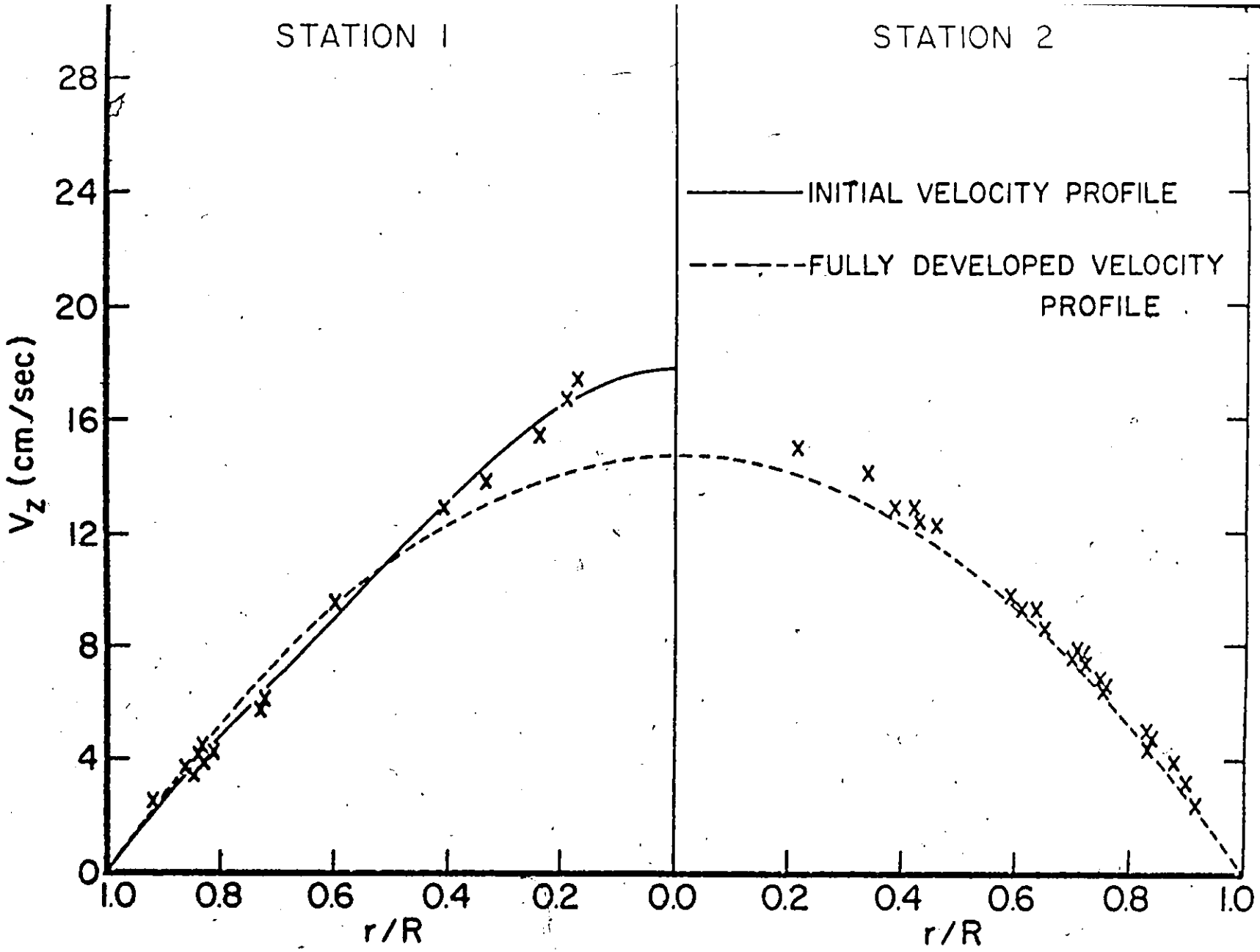

F I G U R E 1 0 VELOCITY PROFILES FOR EXPERIMENT A1

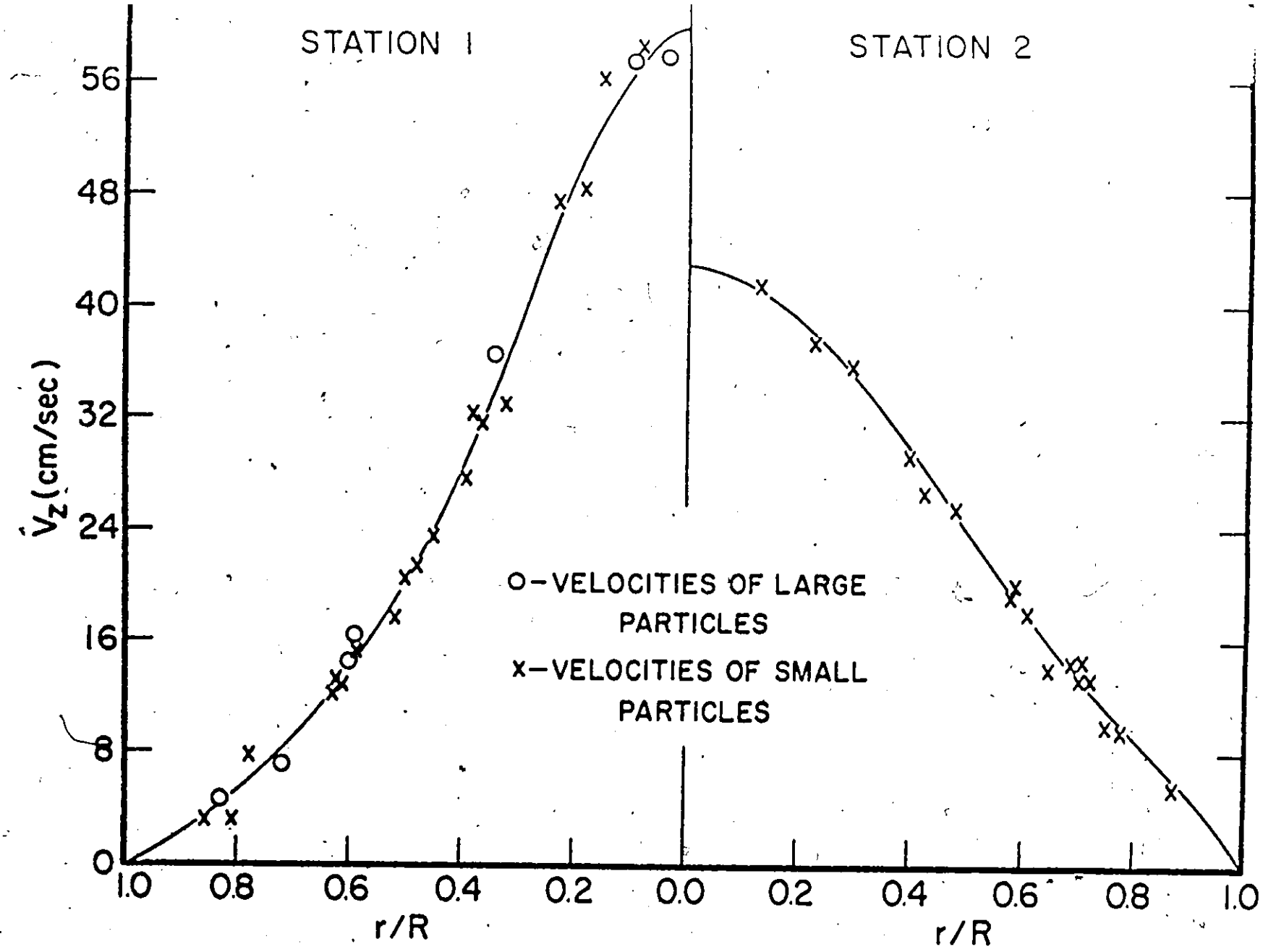

FIGURE 11 VELOCITY PROFILES FOR EXPERIMENT A2

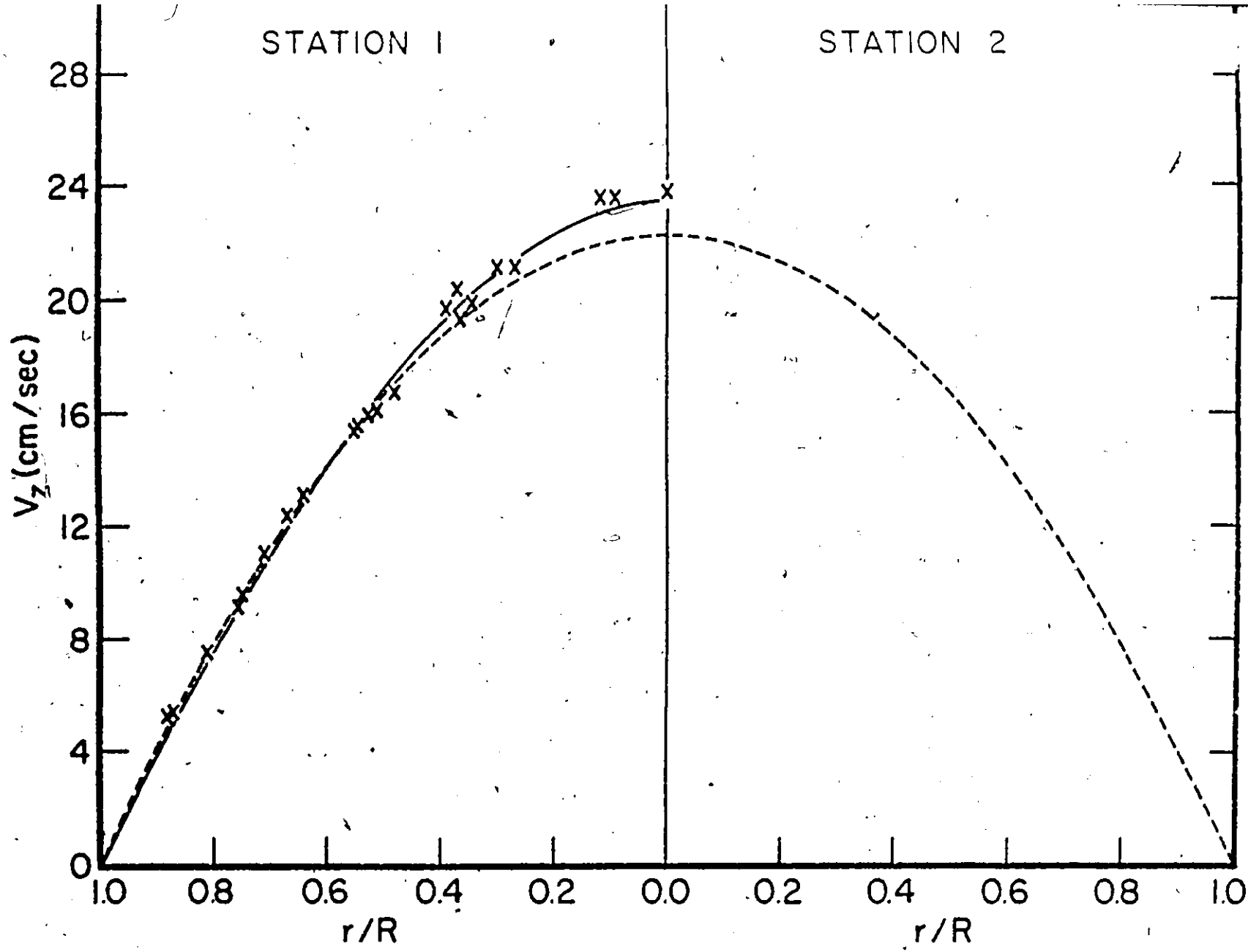

F I G U R E 1 2 VELOCITY PROFILES FOR EXPERIMENT B1

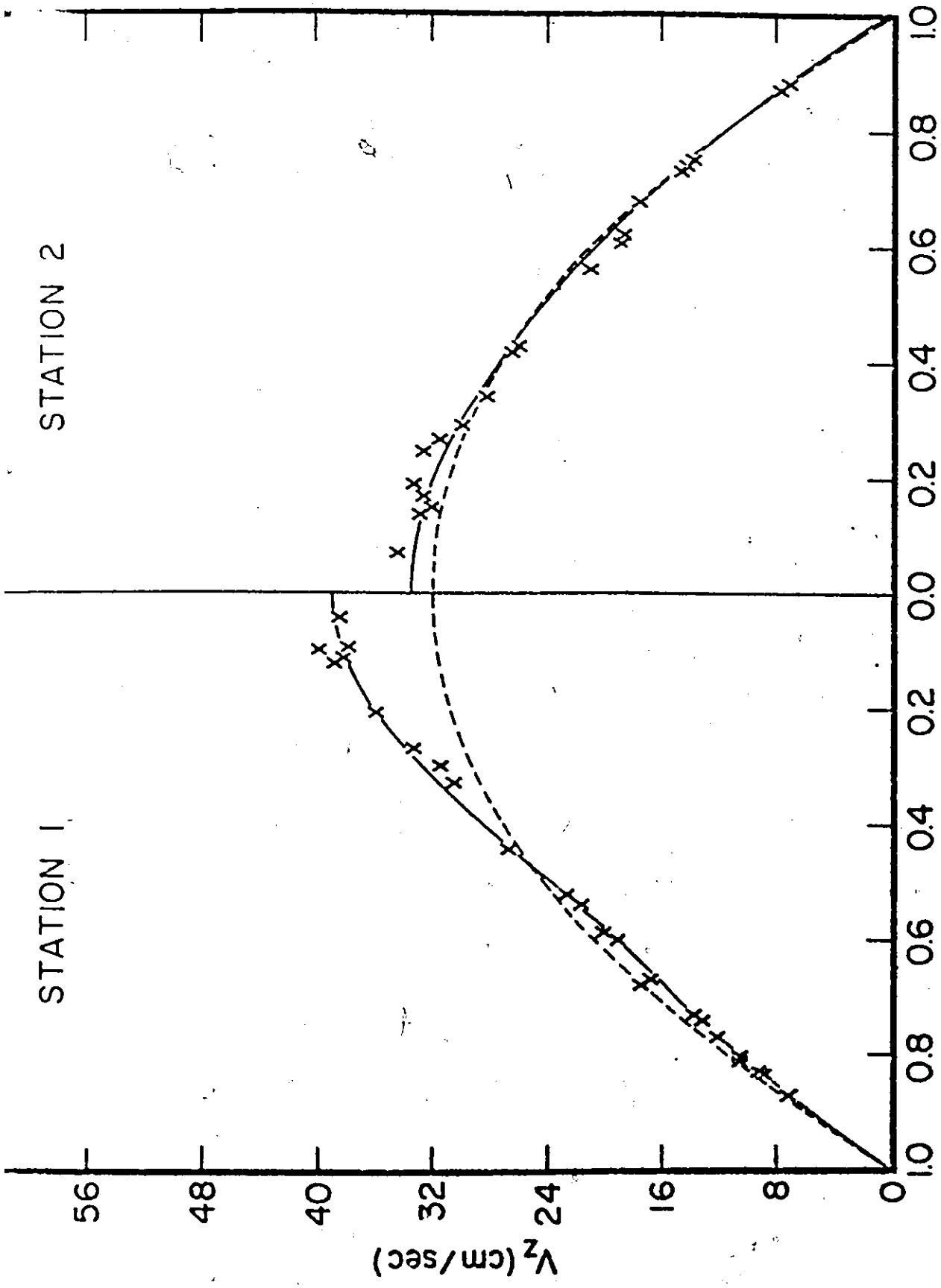

FIGURE 13 VELOCITY PROFILES FOR EXPERIMENT B2

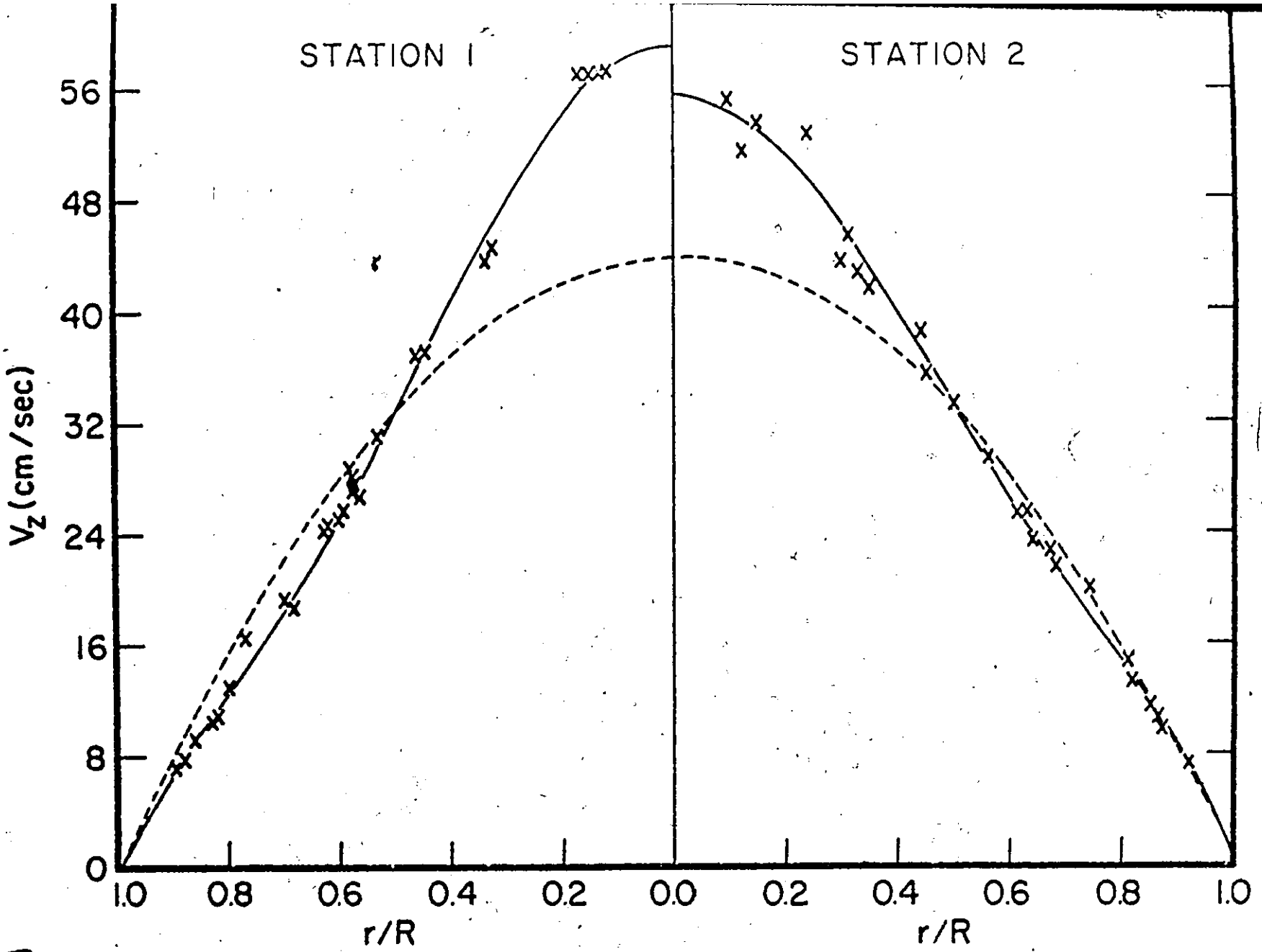

F I G U R E 3 4 VELOCITY PROFILES FOR EXPERIMENT B3

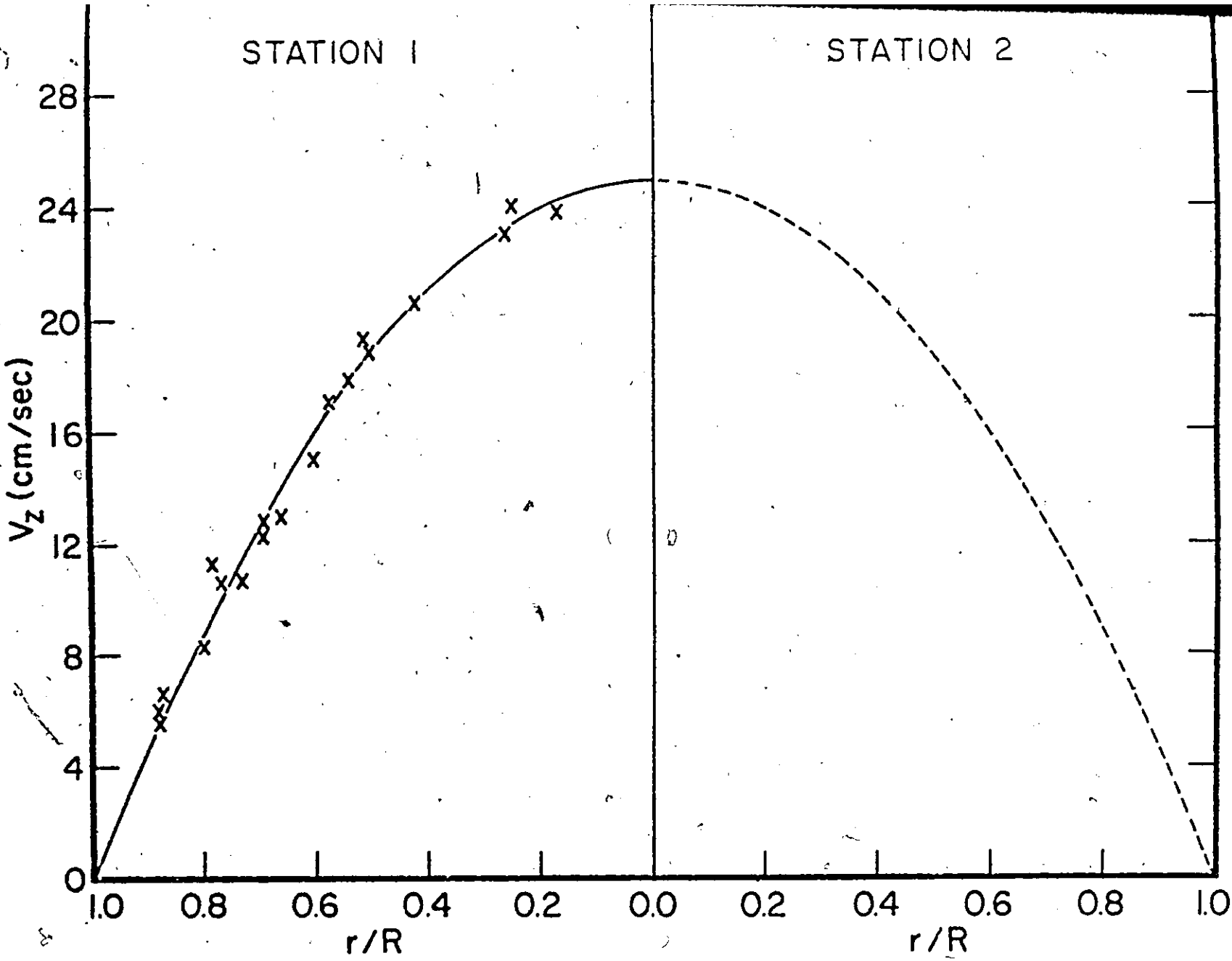

F I G U R E 1 5 VELOCITY PROFILES FOR EXPERIMENT C1

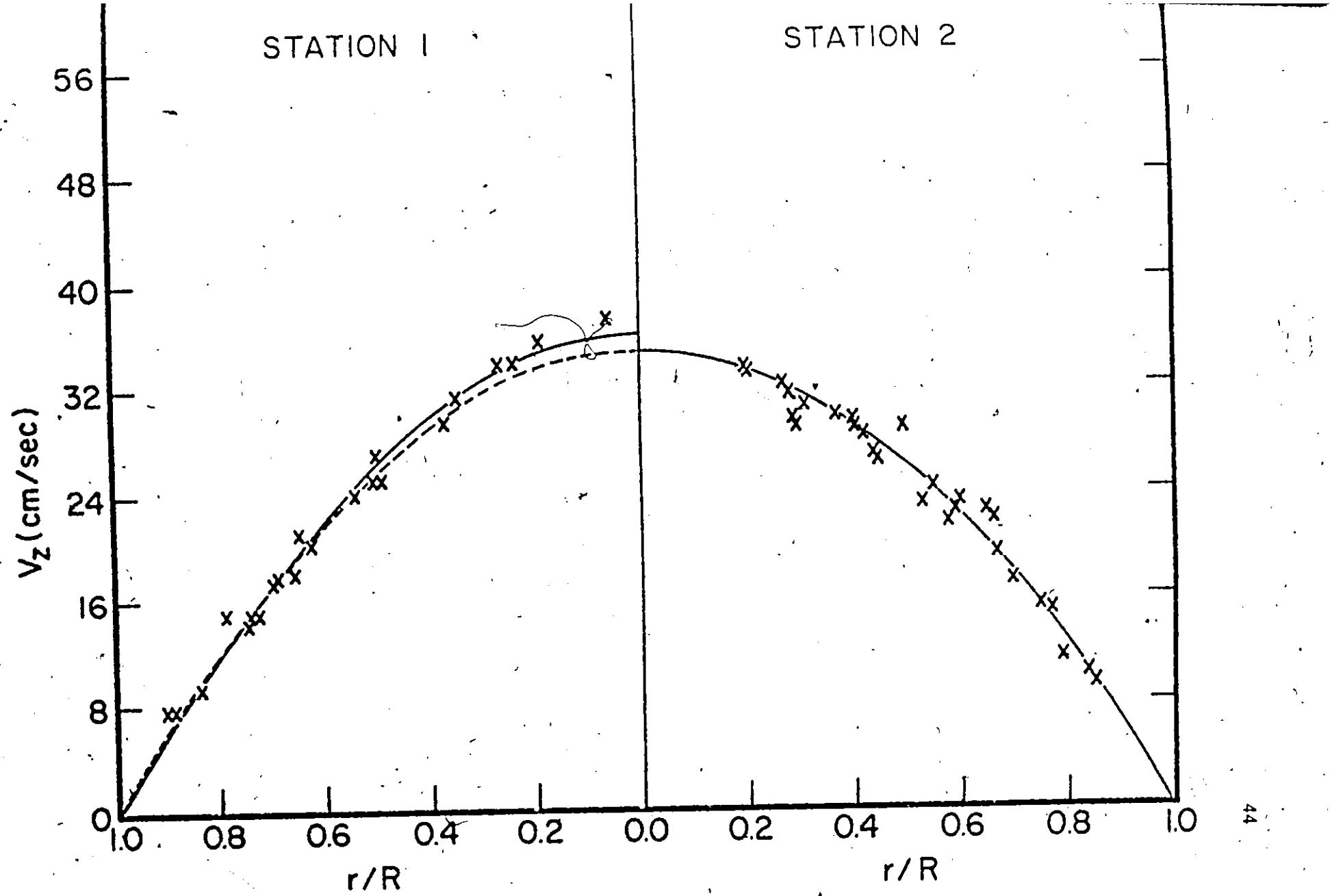

FIGURE 16 VELOCITY PROFILES FOR EXPERIMENT C2

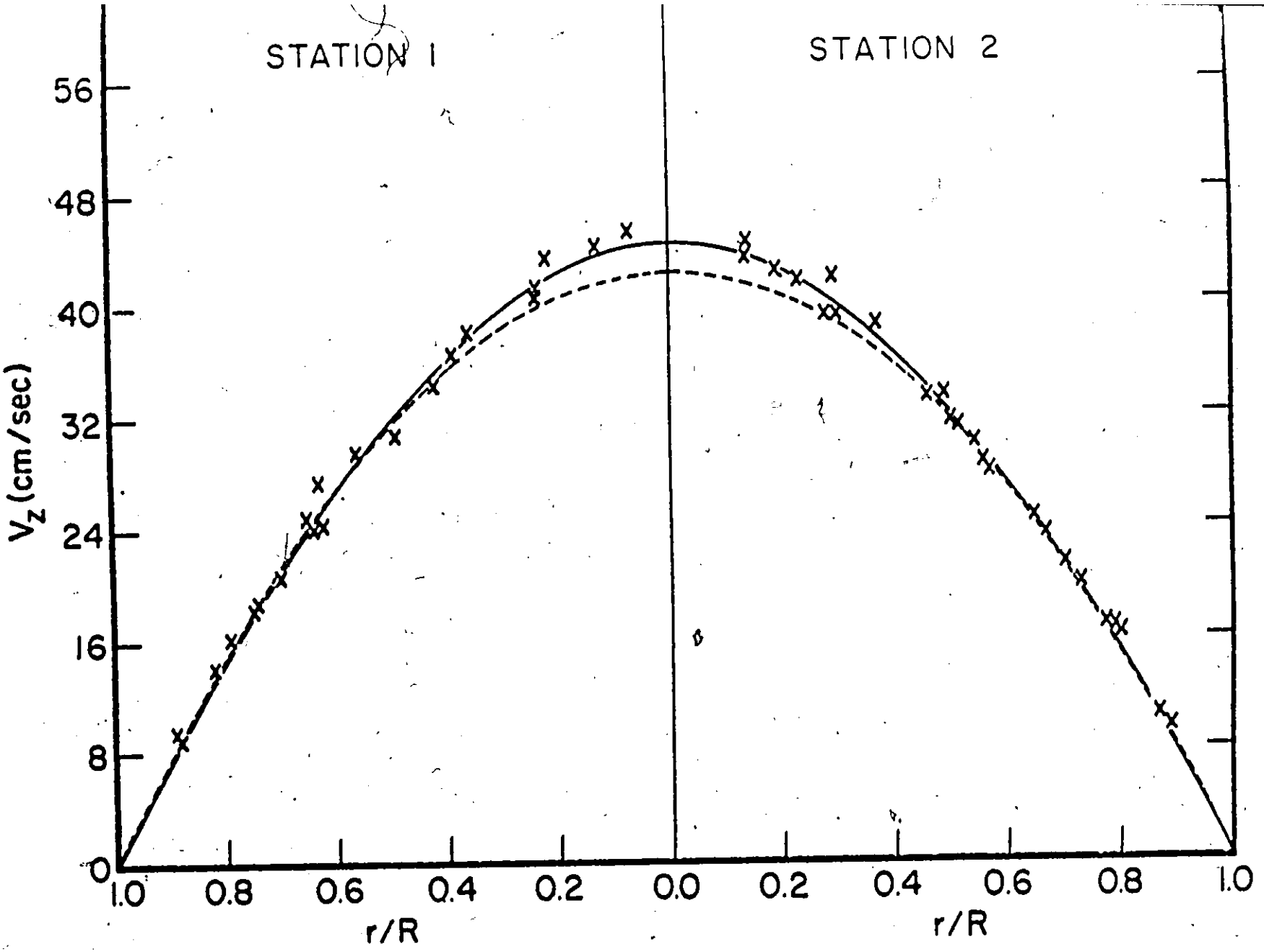

FIGURE 17 VELOCITY PROFILES FOR EXPERIMENT C3

near the centreline were higher for this experiment than for any other experiment. Since velocity values from large particles lie within the scatter band for velocities obtained from small particles, it may be concluded that particle inertia effects are negligible for the range of particle sizes and Reynolds numbers encountered in this series of experiments.

In all but one case the velocity data was reasonably well presented by an even least squares polynomial of degree 4 or 6 (table 12). The upstream velocity profile for experiment A2 was better approximated by a function of the form

$$v_z = 2a_0(1 - \eta^2) + a_1 g_1 + a_2 g_2 + \text{------} a_5 g_5 \qquad (5.1)$$

where

$$g_i = \frac{2}{\alpha_i} \left\{ \frac{J_o(\alpha_i \eta)}{J_o(\alpha_i)} - 1 \right\} \qquad \text{(Equation 2.14)}$$

If the mean velocity, V_m, is computed from

$$V_m = 2 \int_{\eta=0}^{1} v_z \, \eta \, d\eta \qquad \text{(Continuity)} \qquad (5.2)$$

it may be shown, by making use of the orthogonality properties (equation A2.15) that

$$V_m = a_o$$

EXPERIMENT	d/D (h cm.)	T (Degrees C)	μ(centiPoise)	Q(cm^3/sec.)	Re_d	Re_D
A1	0.63 (0.381)	21.0	7.3	22.02	308	194
A2	0.63 (0.381)	22.0	7.1	38.14	548	345
A3	0.63 (0.381)	21.0	7.3	53.94	755	475
B1	0.79 (0.214)	24.2	6.55	22.02	274	216
B2	0.79 (0.214)	22.0	7.1	38.14	437	345
B3	0.79 (0.214)	22.4	7.0	53.94	626	495
C1	0.93 (0.074)	23.0	6.85	22.02	222	207
C2	0.93 (0.074)	23.0	6.85	38.14	385	358
C3	0.93 (0.074)	24.7	6.45	53.94	577	537

T A B L E 1 1 REYNOLDS NUMBERS BASED ON UPSTREAM AND DOWNSTREAM TUBE DIAMETERS

EXPERIMENT	COEFFICIENTS OF NON-DIMENSIONAL VELOCITY PROFILE				z_{max}
	η^0	η^2	η^4	η^6	
$A1_1$	2.402756	-4.574227	4.097885	-1.926415	0.229436
$A1_2$	2.0	-2.0	0.0	0.0	--
$A2_1$	$\omega = 2(1-\eta^2) + a_1 g_1 + a_2 g_2 + \cdots\cdots\cdots + a_5 g_5$				0.380165
$A2_2$	2.706054	-6.111920	5.981294	-2.575434	0.271113
$B1_1$	2.106422	-2.425806	0.319443	0.0	0.118325
$B1_2$	2.0	-2.0	0.0	0.0	--
$B2_1$	2.406817	-4.763155	4.628175	-2.271858	0.238799
$B2_2$	2.094210	-2.377005	0.282877	0.0	0.109785
$B3_1$	2.697008	-6.268051	6.531145	-2.960121	0.272145
$B3_2$	2.449219	-5.115303	5.302998	-2.636935	0.250565
$C1_1$	2.0	-2.0	0.0	0.0	--
$C1_2$	2.0	-2.0	0.0	0.0	--
$C2_1$	2.081727	-2.327288	0.245751	0.0	0.099181
$C2_2$	2.0	-2.0	0.0	0.0	--
$C3_1$	2.095125	-2.380629	0.285567	0.0	0.110086
$C3_2$	2.076011	-2.304138	0.228176	0.0	0.093944

TABLE 12 NON-DIMENSIONAL FORM OF VELOCITY PROFILE AND MAXIMUM VALUE OF Z.

and equation (5.1) may be written in non dimensional form as

$$\omega = 2(1 - \eta^2) + a_1' g_1 + a_2' g_2 + \text{-----} a_5' g_5 \qquad (5.3)$$

with $a_1' = a_1 / a_o$ etc.

In this case, since

$$\omega = \omega_{f.d.} + \omega^* \quad \text{for all } Z \qquad \text{(equation 2.8)}$$

and

$$\omega^* \Big|_{Z=0} = \sum_{i=1}^{\infty} c_i g_i \qquad \text{(equation 2.13)}$$

It follows, either by comparing terms directly or by using equation A2.20 together with A2.14, that the coefficients, c_i, are given by

$$\begin{aligned} c_i &= a_i' \qquad 1 \leq i \leq 5 \\ c_i &= 0 \qquad\quad i > 5 \end{aligned} \qquad (5.4)$$

For the cases treated by polynomials, the non-dimensional form of the curve was obtained by dividing throughout by the mean velocity computed from equation 5.2. With this as upstream boundary condition to equation 2.10, continuity was automatically satisfied within the mathematical solution, the non-dimensional centreline velocity tending to an equilibrium value of 2.

The mean velocities calculated by means of equation 5.2 were found to be within 12% of the corresponding values given by Q/A, where the flow-rates, Q, were obtained from figure 6 and A is the cross-sectional area

of the tube.

This curve gives the theoretical flowrate (from continuity and the Bernoulli equation) for a venturimeter with a throat to main diameter ratio of 0.303. An independent calibration was carried out using water (specific gravity 1 c.f. 1.04 for suspending fluid) in an open system, the flowrate being measured with the aid of a stopwatch and a large graduated cylinder. Values obtained in this way were within 3% of those given by the theoretical curve. The large discrepancy between the theoretical flowrates and those from equation 5.1 is explained by the fact that camera filming speeds were lower than anticipated. Great difficulty was encountered in obtaining timing pulses on the side of the film. This would have allowed the filming speed to be determined to within 1.0% whereas the speed regulator was only accurate to ±5%. However, for the purpose of determining development lengths, this is of no consequence since the maximum value of the non-dimensional axial parameter Z, given in table 12, is dependent only upon the shape of the initial velocity profile. The partial development length, z, measured from the axial location of the initial velocity profile is then given by

$$z = Z. \ Re_D \ . \ R \ / \ 2 \qquad (5.5)$$

The generation of a set of velocity profiles from equation (2.13) is illustrated for two different upstream boundary conditions. With equation (5.3) as upstream boundary condition, a set of velocity profiles

was generated from the equation

$$\omega = 2(1 - \eta^2) + \sum_{i=1}^{\infty} c_i g_i e^{-\alpha_i^2 Z^*} \quad \text{(equation A2.17)}$$

and are presented in figure 18. Figure 19 shows a similar set of curves for the case of an input profile with non-dimensional centreline velocity less than 2. Also presented for each of the above cases is the graphical form of the relationship between the stretching factor, ϵ, and the stretched coordinate, Z^*, both of which appear to tend to an asymptotic limit of about 1.83 (in this figure the curves have been truncated at a value of Z^* corresponding to a non-dimensional centreline velocity of about 2.04). For the decreasing centreline velocity case, the maximum value of Z was obtained by numerically integrating under the ϵ versus Z^* curve up to a value of Z^* corresponding to $\omega_c = 2.02$ i.e. up to the point where the centreline velocity was within 1% of the equilibrium value ($2 V_m$).

Table 13 lists the partial development lengths, z_1 and z_2, that were obtained by using the experimentally determined velocity profiles at stations 1 and 2 as upstream boundary conditions to equation 2.10. The development length, L, measured from the step, was taken as $(z_1 + 25)$ cm. The percentage differences listed in the fourth column were computed as

$$\% \text{ Difference, } \delta = \frac{| 12.7 - (z_1 - z_2) |}{z_1} \qquad (5.6)$$

i.e. the absolute value of the difference between the true distance from station 1 to station 2 and the predicted distance $(z_1 - z_2)$, expressed as

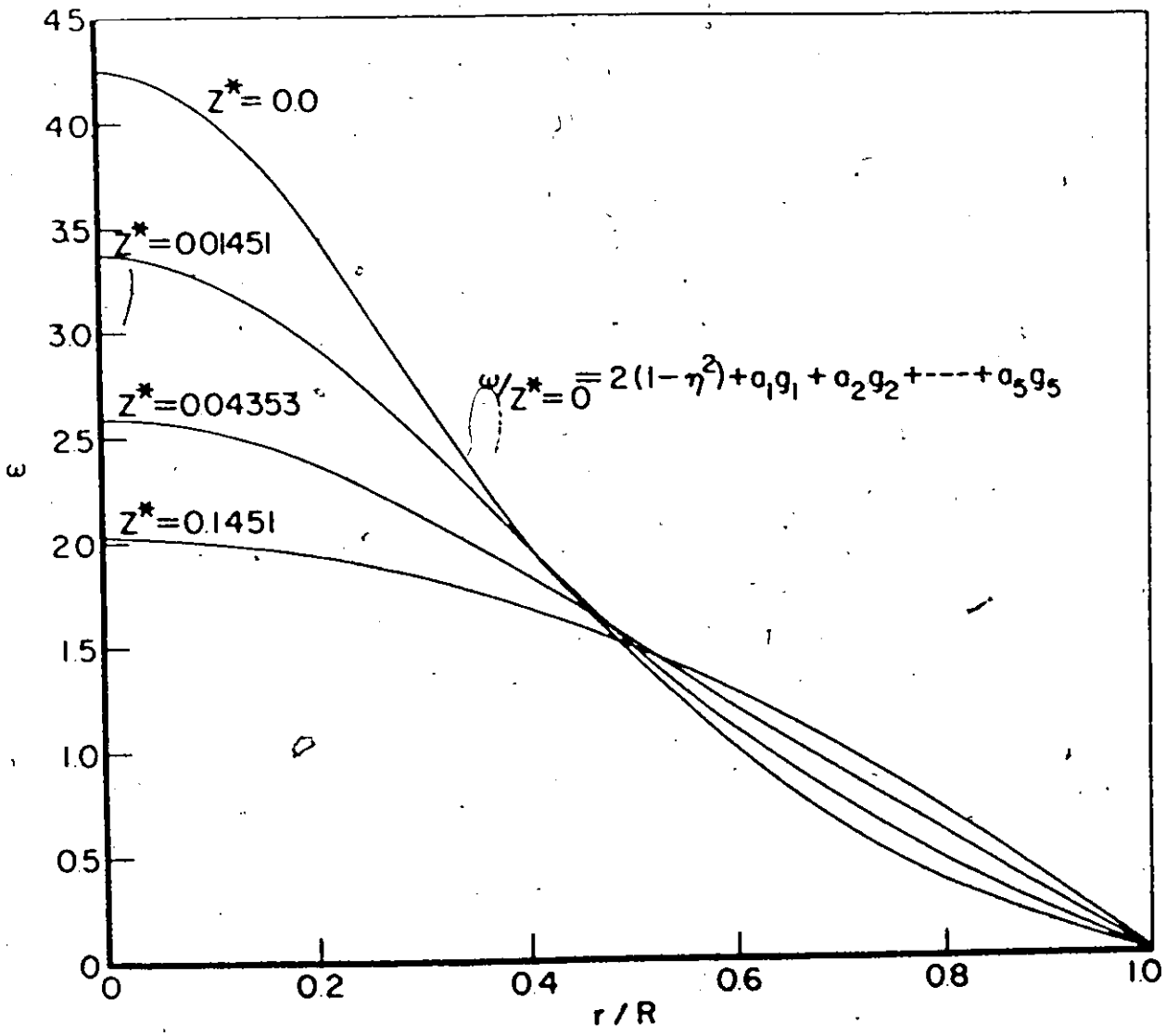

FIGURE 1P - MATHEMATICALLY GENERATED SEQUENCE OF VELOCITY PROFILES WITH DECREASING CENTRELINE VELOCITY

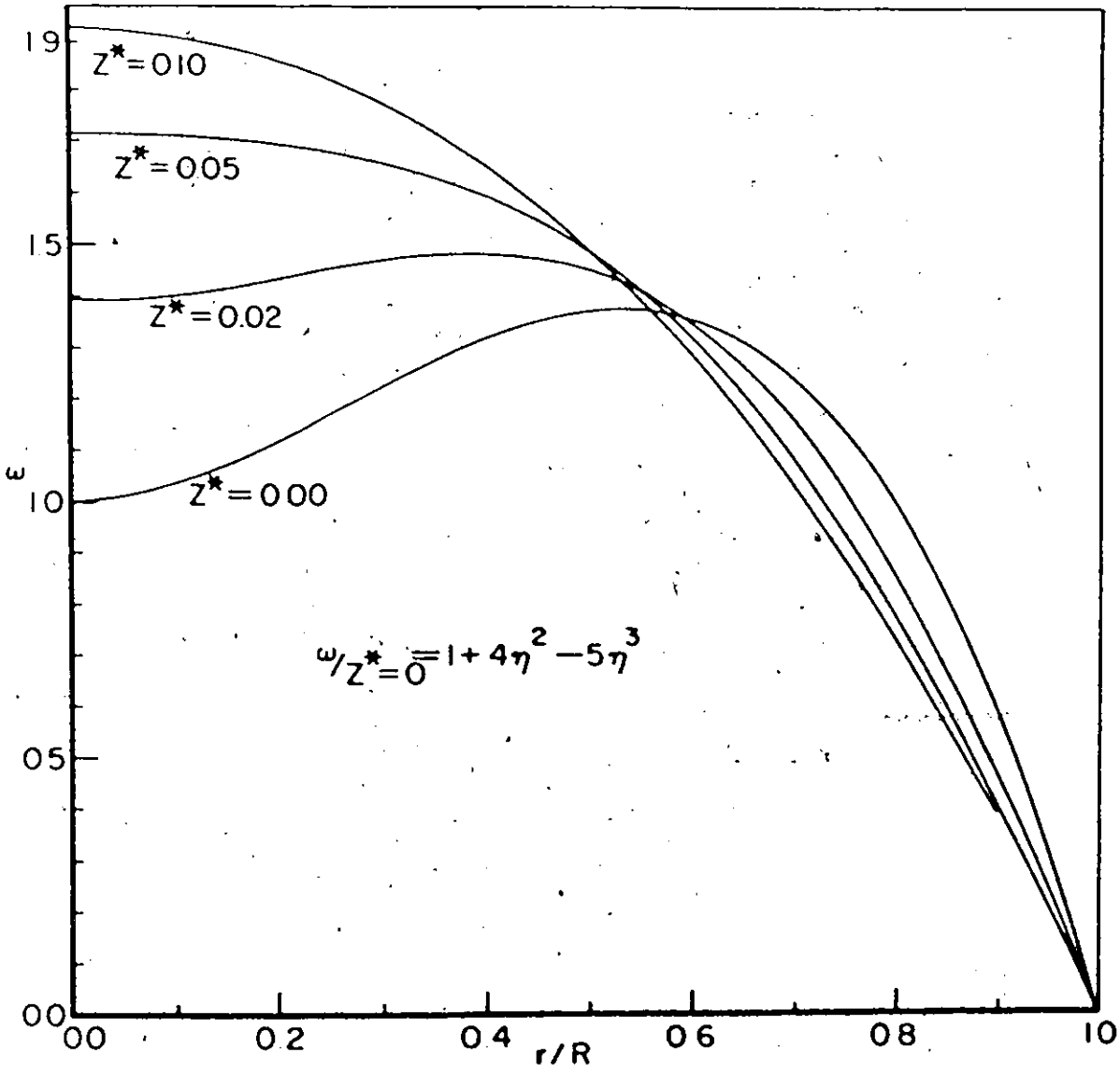

FIGURE 19 - MATHEMATICALLY GENERATED SEQUENCE OF VELOCITY PROFILES WITH INCREASING CENTRELINE VELOCITY

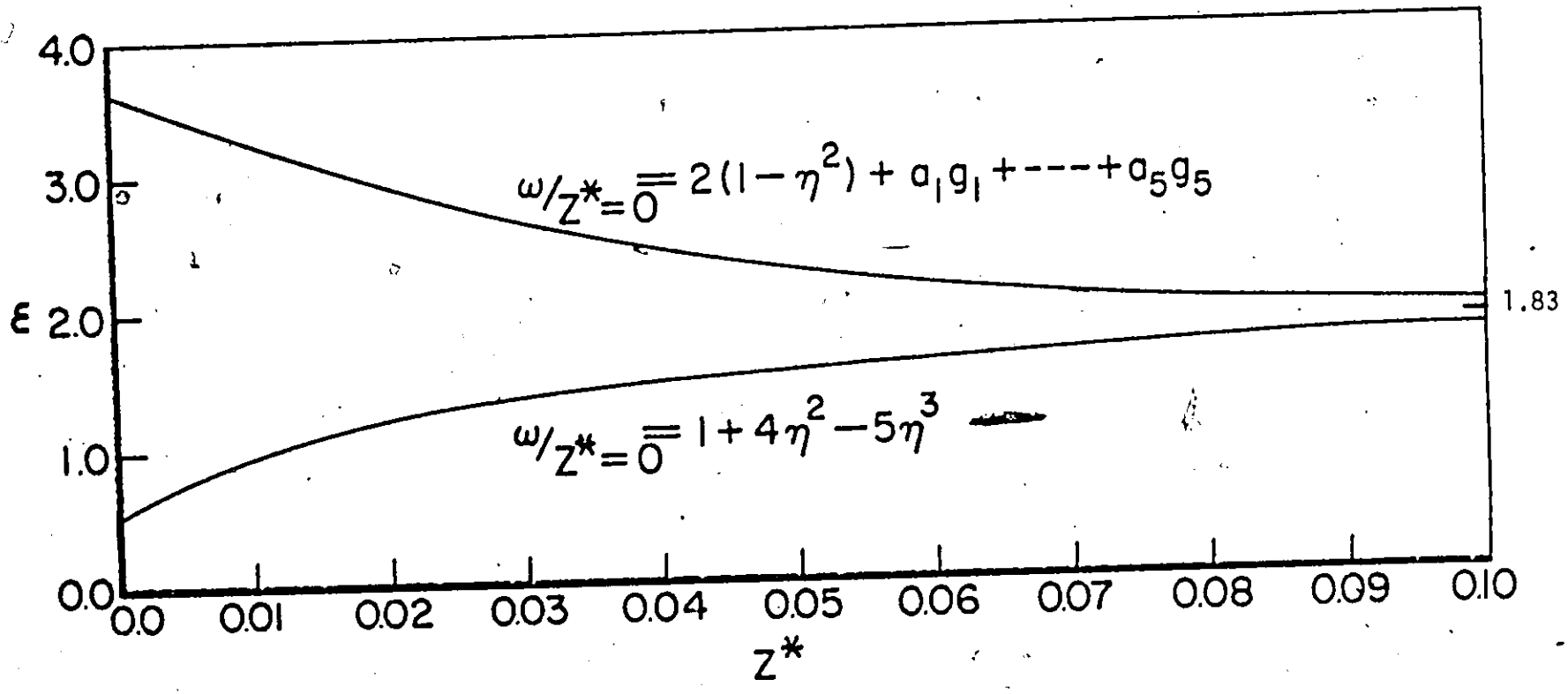

FIGURE 20 STRETCHING FACTOR ε VERSUS STRETCHED COORDINATE Z^* FOR CURVES OF FIGURES 18 and 19

EXPERIMENT	z_1 (cm.)	z_2 (cm.)	L (cm.)	% DIFFERENCES
A1	22.9		47.9	
A2	67.5	48	92.5	10.1
B1	13.1		38.1	
B2	42.6	19.6	67.6	24.2
B3	69.4	63.7	94.4	10.1
C1			$\leq$25.0	
C2	18.3		43.3	
C3	30.4	26.0	51.0	27.3

TABLE 13 DEVELOPMENT LENGTHS

a percentage of the distance z_1. This is not the same as the true error in z, but provides an indication of the relative magnitude of the error from one experiment to the next. Where no value is presented for δ, it was found that all approximating polynomials, up to and including a sixth degree polynomial, gave a non-dimensional centreline velocity of less than 2.02. It is probable that the velocity profile was not quite fully developed, but that the difference between the actual value of ω_ℓ and the fully developed value was quite small. Considering that the difference velocity, ω^*, decreases exponentially and that the flow here was very nearly fully developed, it is conceivable that the length of transition required to accomodate the corresponding centreline velocity change might be of the order of several centimetres.

The smallest values of δ were obtained from velocity profiles which had non-dimensional centreline velocities greater than 2.4. Recalling the approximation by which the inertia terms in the axial Navier-Stokes equation have been linearized, viz.

$$\frac{D}{Dt} v_z \doteq \epsilon(z) V_m \frac{\partial v_z}{\partial z} \qquad (5.7)$$

it is evident that if $|v_z \partial v_z / \partial z| >> |v_r \partial v_z / \partial r|$, which is the case for a high Reynolds number flow, provided also that the axial rate of change of velocity is greater than the velocity gradient, $\partial v_z / \partial r$, then the linearization is quite valid. Upstream, in the region of the centre of the tube, where both v_r and $\partial v_z / \partial r$ are small, the approximation is good.

On the tube wall equation (5.7) holds well because v_z and v_r are both zero. It is not strictly valid in the annular region just away from the wall. Figure 20 indicates a decrease in the value of ϵ with increasing Z, and this is to be expected since ϵ is a weighting factor applied to the mean velocity, V_m, and the velocity is decreasing in the central region of the tube. For the case of an increasing centreline velocity (figure 19), the velocity gradient in the central region is always small. This is similar to the case of a uniform entry profile, where an inviscid core flow in the centre of the tube gradually tapers off in the z direction as the annular boundary layer surrounding it thickens. Here, since the velocity increases in the z-direction and the linearizing approximation (equation 5.7) is good because $\partial v_r/\partial z$ is zero, the stretching factor, ϵ, increases with Z.

Where the percentage difference, δ (and hence the error) is large, the explanation lies in the fact that the magnitude of the second inertia term, $v_r \partial v_z/\partial r$, is of greater significance than in the previous cases. It should be mentioned that although the term $\Lambda(z)$ may include the residual of the inertia terms which is a function of the axial coordinate (8), both v_r and $\partial v_z/\partial r$ are strong functions with respect to r, the former being zero at the centre and at the wall and attaining some maximum in between, and the latter being zero at the centre and attaining a maximum value between the centre and the wall. The larger the initial non-dimensional centreline velocity, the smaller the resulting percentage error.

Provided that the corresponding station is far enough downstream from the reattachment point, the radial velocity component, v_r, is still small compared with the axial component, v_z. The films that were taken did not indicate an appreciable radial velocity component at station 1 (the particles moved parallel to the tube axis).

A correlation was obtained for development length, L, as

$$L/D = K\, Re_D^m \quad [\, 1 - (d/D)^n \,] \tag{5.8}$$

This is a simple functional form which leads to a value for L/D of zero when d/D is unity. This must be the case since the flow upstream of the step is already fully developed. A non-linear least squares curve fitting program using Marquardt's Maximum Neighborhood Method was used to obtain the values of the three unknowns in the above equation. This yielded

$$K = 0.27$$

$$m = 0.94$$

$$n = 2.77$$

with the sum of squares of residuals equal to 152.4, the r.m.s. value equal to 6.17 and the largest residual 8.62 for an observed L/D of 21. It is to be expected, from the magnitude of the percentage difference, δ (table 13), that this data point is rather inaccurate. The preceding value in table 13 was omitted because it was not possible in this case to make an estimation of development length.

5.2 THE VORTEX REGION

With an increased particle concentration in the flow, observations were made of vortex length for the case of a 0.63 diameter ratio expansion (since this produced the largest vortices). The reattachment length was determined by noting the farthest distance that a particle would travel from the step before turning back and moving upstream again. In figure 21 the reattachment length in step heights is plotted as ordinate against the upstream Reynolds number. This allows direct comparison to be made with the results of Back and Roschke (2) which were obtained for a tube diameter ratio of 0.385 and for upstream Reynolds numbers of 20 to 4200. It should be stated here that for the latter case the velocity profile in the smaller diameter tube was uniform and not parabolic as for the present experiment. The curve must pass through, or at least very close to the origin and hence its slope increases slightly over the lower Reynolds number range, but is fairly uniform over its latter portion (Re_d between 600 and 1000). The value of the slope of the straight line which is the best fit to the last 6 points was found to be 0.1187, compared with a value of 0.11 for the linear portion of the curve obtained by Back and Roschke (2). All 8 data points (including 0,0) were correlated by the equation

$$\frac{x_R}{h} = 0.048\ Re_d^{1.1} \qquad (5.9)$$

the residual sum of squares here being 44 and the residual root mean square 2.7. It is interesting to note that, as with the development length

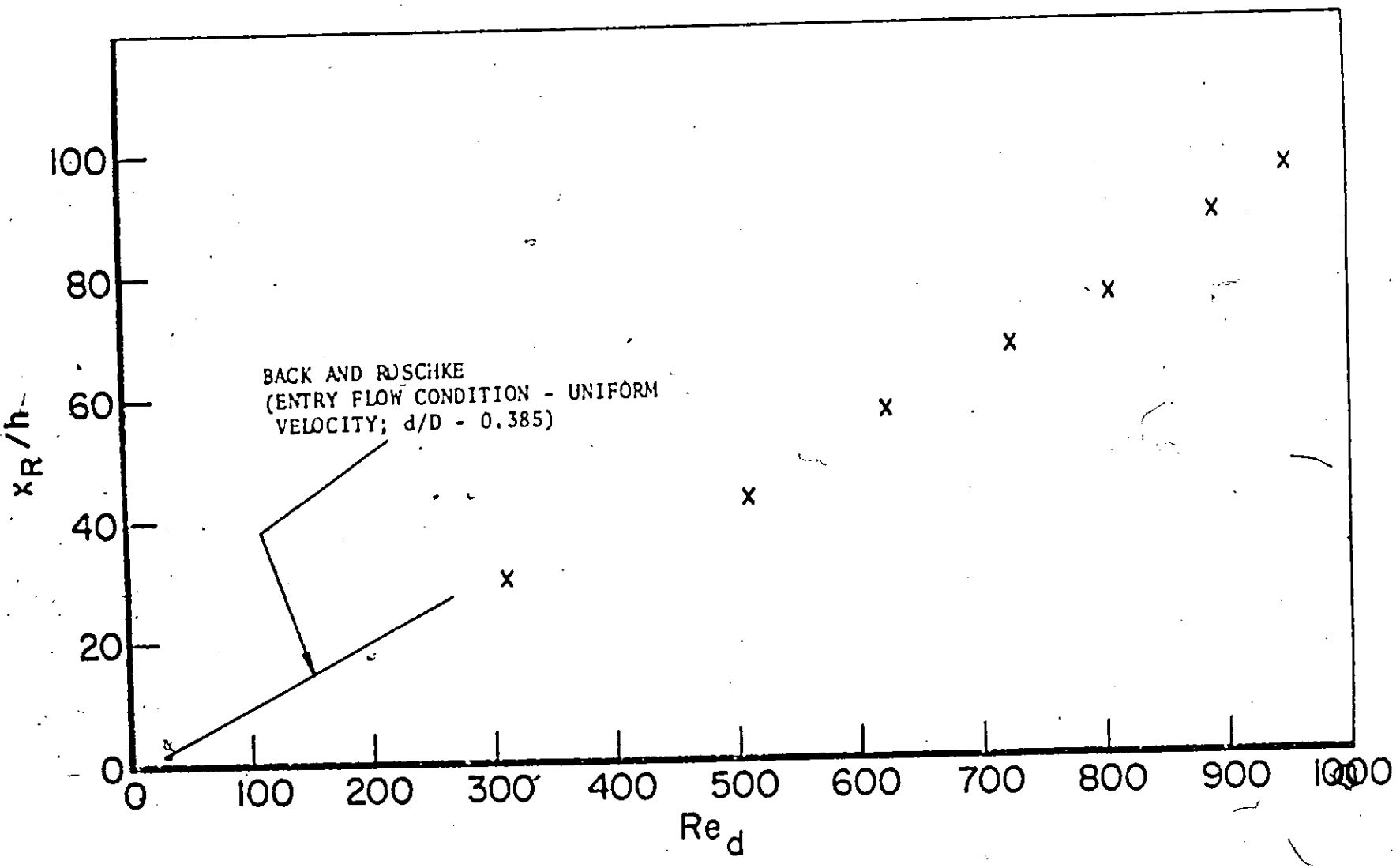

F I G U R E 21 REATTACHMENT LENGTH VERSUS UPSTREAM REYNOLDS NUMBER FOR A TUBE DIAMETER RATIO OF 0.63

correlation, the exponent of the Reynolds number is approximately unity. Whereas the above authors discovered the onset of instability at a Reynolds number of 250, marking the attainment of a maximum vortex length of 25 step heights, it was found in the present case that an unstable flow regime was encountered at a value of upstream Reynolds number of 1090 which corresponded to a vortex length of 113 step heights.

The reverse-flow region extended beyond the area in which instability, in the form of periodic turbulent pulsing, was first observed to occur. As the Reynolds number was increased the turbulent pulsing became more random in nature and the region of onset of instability moved back towards the step. It was very difficult here to define a reattachment point. At an upstream Reynolds number of 1560, only the first 10 cm (27 step heights) beyond the step was free from turbulent instability.

CONCLUSIONS

A flow visualisation technique has been developed which allows fluid velocities to be determined by photographically recording the motion of small, neutrally buoyant tracer particles with the aid of a high speed movie camera.

Using this technique, the laminar flow downstream of an abrupt, circular channel expansion was studied for the case of fully developed Poiseuille flow upstream of the step. Experiments were carried out with tube diameter ratios of 0.63, 0.79 and 0.93 and Reynolds numbers (based on upstream diameter) between 222 and 755. Velocity profiles were obtained at each of two different stations downstream of the reattachment point.

These velocity profiles were used as upstream boundary conditions for the linearized axial Navier - Stokes equation for the purpose of predicting development lengths. When the non-dimensional centreline velocity of the initial velocity profile is greater than 2.4, development length values may be obtained to an accuracy of 10%. Values obtained over the above range of Reynolds numbers and tube diameter ratios were correlated by the equation

$$L/D = 0.27\, Re_D^{0.94} \left[1 - (d/D)^{2.77} \right]$$

With an increased particle concentration in the flow, direct measurements were made of vortex length for a tube diameter ratio of 0.63. The gradient of the flat portion of the curve relating non-dimension re-

attachment length, x_R/h and upstream Reynolds number, Re_d was found to be 0.1187. This agrees well with the value of 0.11 from the work of Back and Roschke (2) for a tube diameter ratio of 0.385. A correlation was obtained for the whole laminar region as

$$x_R/h = 0.048\ Re_d^{1.1}$$

Hence both vortex length and development length increase almost linearly with Reynolds number.

REFERENCES

(1) Macagno, E.O. and Hung, T. K., "Computational and Experimental Study of a Captive Annular Eddy", Journal of Fluid Mechanics, Vol. 28, Part I, 1967, pp. 43-64.

(2) Back, L. H. and Roschke, E. J., "Shear-Layer Flow Regimes and Wave Instabilities and Reattachment Lengths Downstream of an Abrupt Circular Channel Expansion", Journal of Applied Mechanics, Sept. 1972, pp. 677 - 681.

(3) Zemanick, P. P. and Dougall, R. S., "Local Heat Transfer Downstream of Abrupt Circular Channel Expansion", Journal of Heat Transfer, Trans. ASME, Series C, Vol. 92, No. 1, Feb. 1970, pp. 53 - 60.

(4) Goldstein, S., "Modern Developments in Fluid Mechanics", Vol. 1, Clarendon Press, Oxford, England, 1938, pp. 304 - 308.

(5) Schiller, L., "Die Entwicklung der laminaren Geschwindigkeitsverteilung und ihre Bedeuturg fur Zahigkeitsmessungen", Zeitschrift fur angewandte Mathematik und Mechanik, Vol. 2, 1922, pp. 98 - 106.

(6) Langhaar, H. L., "Steady Flow in the Transition Length of a Straight Tube", Journal of Applied Mechanics, June 1942, pp. 55-58.

(7) Slezkin, N. A., "Dynamics of Viscous Incompressible Fluids", (in Russian), Gostekhizdat, Moscow, Russia, 1955.

(8) Sparrow, E. M., Lin, S. H. and Lundgren, T. S., "Flow Development in the Hydrodynamic Entrance Region of Tubes and Ducts", The Physics of Fluids, Vol. 7, number 3, March 1964, pp. 338 - 347.

(9) Lew, H. S. and Fung, Y. C., "Entry Flow into Blood Vessels at Arbitrary Reynolds Number", J. Biomechanics, Vol. 3, 1970, pp. 23-38.

(10) Segre, G. and Silberberg, A., "Behaviour of Macroscopic Rigid Spheres in Poiseuille Flow", J. Fluid Mechanics, Vol. 14, 1962, pp. 136-157.

(11) Karnis, A., Goldsmith, H. L. and Mason, S. G., "The Flow of Suspensions through Tubes", Can. J. Chem. E., August 1966, pp. 181 - 193.

(12) Jeffrey, R. C. and Pearson, J. R. A., "Particle Motion in Laminar Vertical Tube Flow", J. Fluid Mechanics, Vol. 22, Part 4, pp.721-735.

(13) Saffman, P. G., "The Lift on a Small Sphere in a Slow Shear Flow", J. Fluid Mechanics, vol. 22, Part 2, pp. 385 - 400.

(14) Simha, R., Kolloid Z., 76, 16 (1936).

APPENDIX I

PARTICLE INERTIA EFFECTS

It is necessary to consider the accuracy with which a small element of the fluid continuum may be represented by a solid, spherical particle of finite size. It is known that the shear stress distribution at the solid/liquid interface, together with the particle's own inertia, results in a radially directed force causing the particle to migrate, in a fully developed Poiseuille flow, to an equilibrium position at about 0.6 x tube radius and that this occurs even under neutrally buoyant conditions. The equilibrium position has been observed to remain constant, except for very small tube Reynolds numbers [$2V_{mean}\,R/\nu$], with both tube Reynolds number and particle/tube diameter ratio, P (10). At tube Reynolds numbers $\leq$ 1.1, the equilibrium position appears to vary with P (11).

The theoretical work available at present provides some insight into the reason for particle migration away from the wall, but there is, as yet, no theory which is able to explain completely the two-way migration observed in Poiseuille flow. Segre and Silberberg (10) have demonstrated that the origin of the forces causing radial displacements is in the inertia of the fluid, and that a particle moves along that part of a unique trajectory which leads from its initial position to its equilibrium position such that, for a given Re_T and P, the radial force causing displacement is a function of radial location only. Correlation of the experimental results, for Reynolds numbers between 2 and 30, indicates

that the transverse velocity is directly proportional to P^3.

Jeffrey and Pearson (12) have obtained correlation of their results, for Reynolds numbers up to 80, by plotting the dimensionless parameter $\overline{V}_r$ $(Re_T)^{-1/2}$ P^{-2} against η, where

$$\overline{V}_r = v_r \text{ (the radial migration velocity)} / v_o \text{ (the centre-line velocity)}$$

and

$$\eta = r/R.$$

The theoretical solution due to Saffman (13), for the case of a spherical particle in a uniform simple sheared flow, tends to support the above correlation. Saffman's analysis takes into consideration only one effect of the presence of the particle walls i.e. that the additional drag caused by the walls makes the particle lag behind the fluid. The second effect, which is ignored for the sake of simplicity, is that the flow field in the vicinity of the particle is altered by the presence of the walls. The expression derived for particle migration velocity may be written as follows:

$$V_r = \frac{k v_s}{3\pi} \left(\frac{V_m r a^2}{\nu R^2} \right)^{1/2} \qquad (1)$$

where k is a constant, a is the particle radius and v_s is the fluid/particle slip velocity. Introducing the expression derived by Sinha (14) for slip velocity

$$| v_s | = 4/3\ V_m P^2 + O\ [P]^3 \qquad (2)$$

and substituting this into equation (1) with the assumption that P is small, so that only the leading termin (2) need be considered, there results

$$v_r = \frac{2\sqrt{2k}}{9\pi} V_m P^3 Re_T^{1/2} \left(\frac{r}{R}\right)^{1/2} \qquad (3)$$

which appears to substantiate the empirical correlation of Jeffrey and Pearson in terms of tube Reynolds number, although the exponent of P suggests a greater increase of radial migration velocity with particle/tube diameter ratio than was observed by the above authors.

A criterion for determining whether the deviation from fluid behaviour is significant may be developed on the basis of the relationship between v_r and P. Firstly, as P tends to zero, v_r does likewise irrespective of the value of Re_T. It is assumed that v_r increases monotonically with respect to P in the case of steady flow with local spatial acceleration components, as well as for a fully developed Poiseuille flow. Suppose that at some point, A, on a streamline where the fluid velocity is v, two particles, having a diameter ratio of at least 2:1, have velocity vectors $\underline{s}_1$ and $\underline{s}_2$. Departure from fluid velocity is brought about by two components; v_s, the slip velocity parallel to the tangent at A, which reduces the magnitude of the vector, and v_r, the radial migration velocity, which produces the angular deviation. If the angle between the two vectors is small, i. e. $(v_{r_1} - v_{r_2})$, then it follows from a consideration of the relationship between v_r and P that both vr_1 and vr_2 are close to the origin. Hence, if v_r is directly proportional to v_s, as indicated by

mation (1), then $\underline{s}_1 \simeq \underline{s}_2 \simeq \underline{v}$.

APPENDIX 2

THE SOLUTION TO EQUATION 2.10

$$\frac{\partial \omega^*}{\partial Z^*} = \frac{1}{\eta}\frac{\partial}{\partial \eta}\left(\eta \frac{\partial \omega^*}{\partial \eta}\right) - 2\left(\frac{\partial \omega}{\partial \eta}\right)_{\eta = 1} \tag{2.10}$$

It is assumed that the solution has the form

$$\omega^* = g(\eta) \cdot N(Z^*) \tag{A2.1}$$

Hence

$$\left.\begin{aligned} \frac{\partial \omega^*}{\partial Z^*} &= g(\eta)\frac{\partial N}{\partial Z^*} \\ \frac{\partial \omega^*}{\partial \eta} &= N(Z^*)\frac{\partial g}{\partial \eta} \end{aligned}\right\} \tag{A2.2}$$

and equation 2.10 becomes

$$g\frac{\partial N}{\partial Z^*} = \frac{N}{\eta}\frac{\partial}{\partial \eta}\left(\eta \frac{\partial g}{\partial \eta}\right) - 2N\left(\frac{\partial g}{\partial \eta}\right)_{\eta = 1} \tag{A2.3}$$

or, by separation of variables,

$$\frac{1}{N}\frac{N}{\partial Z^*} = \frac{1}{g} \cdot \frac{1}{\eta}\frac{\partial}{\partial \eta}\left(\eta \frac{\partial g}{\partial \eta}\right) - \frac{2}{g}\left(\frac{\partial g}{\partial \eta}\right)_{\eta = 1} \tag{A2.4}$$

Since N (Z*) and g (η) are independent variables, they are both equal to the same constant, say $-\alpha^2$.

$$\frac{1}{N}\frac{dN}{dZ^*} = -\alpha^2$$

has the solution

$$N = c\, e^{-\alpha^2 Z^*} \tag{A2.5}$$

where c is a constant.

Also

$$-\alpha^2 g = \frac{1}{\eta}\frac{d}{d\eta}\left(\eta \frac{dg}{d\eta}\right) - 2\left(\frac{dg}{d\eta}\right) \quad \eta = 1 \tag{A2.6}$$

However, if $\omega^* = c\, g(\eta)\, e^{-\alpha^2 Z^*}$ is a solution to equation (2.10), then, since the equation is linear, the most general solution is given by

$$\omega^* = \sum_{i=1}^{\infty} c_i\, g_i(\eta)\, e^{-\alpha_i^2 Z^*} \tag{A2.7}$$

where g_i satisfies

$$\frac{d}{d\eta}\left(\eta \frac{dg_i}{d\eta}\right) + \eta\, \alpha_i^2\, g_i = 2\eta\left(\frac{dg_i}{d\eta}\right) \quad \eta = 1 \tag{A2.8}$$

The left hand side of this equation may be obtained from Bessel's equation

$$X \frac{d}{dX}\left(X \frac{d\Omega}{dX}\right) + \left(X^2 - \nu^2\right)\Omega = 0 \tag{A2.9}$$

by making the transformation

$$X = \beta \eta^{\alpha}, \quad \Omega = \eta^{\xi} g_i$$

and putting $\nu = 0$, $\xi = 0$, $\alpha = 1$, $\beta = \alpha_i$

the general solution to equation (A2.8) is then obtained as

$$g_i = A_i \, Jo \, (\alpha_i \eta) + \beta_i \, Y_o \, (\alpha_i \eta) + C_i \qquad \text{(A2.10)}$$

But the second term tends to $- \infty$ as η tends to zero

Therefore

$$g_i = A_i \, Jo \, (\alpha_i \eta) + C_i \qquad \text{(A2.11)}$$

is the only solution which is valid for all η.

On substituting

$$g_i(\eta) = \frac{2}{\alpha_i} \left(\frac{Jo \, (\alpha_i \eta)}{Jo \, (\alpha_i)} - 1 \right) \qquad \text{(A2.12)}$$

into equation (A2.8) it is found that the equation is satisfied provided

$$J_1 \, (\alpha_i) \; / \, J_o \, (\alpha_i) = 0.5 \alpha_i \qquad \text{(A2.13)}$$

The latter equation generates the eigenvalues, α_i, of equation (A2.8) and the g_i are the corresponding eigenfunctions.

The following orthogonality properties may also be verified by substitution:

$$\int_A g_i \, dA = 0 \qquad \text{(A2.14)}$$

$$\int_A g_i \, g_j \, dA = \begin{cases} 0 & i \neq j \\ \pi R^2 & i = j \end{cases} \qquad \text{(A2.15)}$$

It remains to determine the coefficients c_i. The initial velocity profile may be expressed as

$$\omega \Big|_{Z^* = 0} = f(\eta) \qquad \text{(A2.16)}$$

The non-dimensional difference velocity, ω^*, is given by

$$\omega^* = \omega - 2(1 - \eta^2) \qquad \text{(A2.17)}$$

Hence

$$\omega^* \Big|_{Z^* = 0} = \sum_{i=1}^{\infty} c_i \, g_i(\eta) = f(\eta) - 2(1 - \eta^2) \qquad \text{(A2.18)}$$

Multiplying throughout by g_i and integrating over the tube cross-section

$$\sum_{j=1}^{\infty} \int_{\eta=0}^{1} c_j g_i g_j \, \eta \, d\eta = \int_{\eta=0}^{1} f \, g_i \, \eta \, d\eta - 2 \int_{\eta=0}^{1} g_i \, \eta(1 - \eta^2) \, d\eta \qquad \text{(A2.19)}$$

Finally, making use of the properties of the eigenfunctions, g_i, (equation A2.15)

$$c_i = 2 \int_{\eta=0}^{1} f \, g_i \, \eta \, d\eta \div 2/\alpha_i \qquad \text{(A2.20)}$$

APPENDIX 3

DERIVATION OF AN EXPRESSION FOR ϵ

By using the continuity equation, the left hand side of the axial Navier-Stokes equation may be written

$$\frac{\partial}{\partial r}(v_r v_z) + \frac{\partial}{\partial z}(v_z^2) + \frac{v_r v_z}{r}$$

Integrating both sides of the equation over the cross-sectional area of the tube and noting that

$$\int_0^R r \frac{\partial}{\partial r} f(r)\, dr = -\int_0^R f(r)\, dr \qquad (A3.1)$$

with $f(r) = v_r v_z = 0$ on the boundary, we obtain

$$\frac{2}{R^2}\int_0^R r \frac{\partial}{\partial z}(v_z^2)\, dr = \left[g_z - \frac{\partial}{\partial z}\left(\frac{p}{\rho}\right)\right] + \frac{2\nu}{R^2}\int_0^R \frac{\partial}{\partial r}\left(r \frac{\partial v_z}{\partial r}\right) dr \qquad (A3.2)$$

Again using the continuity equation, the mechanical energy equation may be written as follows:

$$\frac{1}{2}\frac{\partial}{\partial z}(v_z^3) + \frac{1}{2}\frac{\partial}{\partial r}(v_z^2 v_r) + \frac{v_r v_z^2}{2r} = v_z\left[g_z - \frac{\partial}{\partial z}\left(\frac{p}{\rho}\right)\right] + \nu v_z\left[\frac{1}{r}\frac{\partial}{\partial r}\left(r\frac{\partial v_z}{\partial r}\right)\right] \qquad (A3.3)$$

As before, the equation is integrated over the tube cross-section and equation (A3.1) introduced, this time with $f(r) = v_r v_z^2$. This yields

$$\int_{r=0}^{R} r \frac{\partial}{\partial z}\left(\frac{v_z^3}{2}\right) dr = \left[g_z - \frac{\partial}{\partial z}\left(\frac{p}{\rho}\right)\right] \int_{r=0}^{R} r\, v_z\, dr + \nu \int_{r=0}^{R} v_z \frac{\partial}{\partial r}\left(r \frac{\partial v_z}{\partial r}\right) dr \qquad \text{(A3.4)}$$

For an exact velocity solution, the term $[g_z - \frac{\partial}{\partial z}(\frac{p}{\rho})]$ would be the same whether obtained from equation (A3.3) or from (A3.4). Equating for this term and rearranging gives

$$\epsilon = \left[\frac{\int_{r=0}^{R} r \frac{\partial}{\partial z^*}\left(\frac{v_z^3}{2}\right) dr - \frac{2}{R^2} \int_{r=0}^{R} r\, v_z\, dr \cdot \int_{r=0}^{R} r \frac{\partial}{\partial z^*}(v_z^2)\, dr}{\nu \int_{r=0}^{R} v_z \frac{\partial}{\partial r}\left(r \frac{\partial v_z}{\partial r}\right) dr - \left[\int_0^R r\, v_z\, dr\right] \frac{2\nu}{R^2} \int_{r=0}^{R} \frac{\partial}{\partial r}\left(r \frac{\partial v_z}{\partial r}\right) dr} \right] \qquad \text{(A3.5)}$$

which may be written in terms of the non-dimensional parameters as follows:

$$c = \frac{\int_{\eta=0}^{1} (2\bar{\omega} - 1.5\,\omega^2)\,\eta\,\frac{\partial\omega}{\partial Z^*}\,d\eta}{\left(\frac{\partial\omega}{\partial\eta}\right)_{\eta=1} + \int_{\eta=0}^{1} \eta\left(\frac{\partial\omega}{\partial\eta}\right)^2 d\eta} \qquad \text{(A3.6)}$$

APPENDIX 4

ESTIMATION OF DISPLACEMENT OF PARTICLE IMAGE DUE TO REFRACTION OF BOUNDING RAYS AT LIQUID/GLASS INTERFACE

The maximum error is incurred for the case of a particle situated close to the tube wall and a bounding ray which is at right angles to the line joining tube axis and particle centre. This ray strikes the tube wall at the largest angle of incidence. For a particle of diameter 300 μ in contact with the tube wall, this angle may be found by a geometrical construction to be 79.^{o}.

Since the radius of curvature of the inner wall is large compared with the wall thickness, t, the angle subtended by the two radii, which intersect the incident and refracted ray at the inner and outer wall respectively, is small and the incident and emergent rays are parallel.

The angle of refraction at the inner wall is given by

$$\frac{\sin i}{\sin r} = {}_{\ell}\mu_{g}$$

where

- i is the angle of incidence at the inner wall
- r is the angle of refraction
- ${}_{\ell}\mu_{g}$ is the index of refraction for a ray travelling from the liquid to the glass

For a compound wall

$$_1\mu_2 = \frac{\mu_2}{\mu_1}$$

Hence $$_\ell\mu_g = \frac{\mu_g}{\mu_\ell} = \frac{1.474}{1.466}$$

For an angle of incidence of 79°, r = 77° and the angle through which the ray is deflected is 2°. The path length is approximately 2t. Hence the image of the particle centre is shifted through about 0.168 mm, or less than 1% of the tube diameter, for the worst case.

APPENDIX 5

ERROR ANALYSIS

The following were measured quantities:

(1) Flowrate

(2) Viscosity of Suspending Fluid

(3) Particle Velocity

(4) Non-dimensional radial coordinate of particle centre (measured directly)

(5) Tube Diameters

Flowrate

Accuracy of Venturimeter Calibration Curve = ± 3%

Maximum Error in Reading Pressure Difference = ± 5%

Total Error in Measuring Flowrate = ± 8%

Viscosity of Suspending Fluid

Maximum Error Incurred in Making a Viscosity Measurement at $T^{o}C$ = 1% of Full Scale Reading = ± 0.1 cP

Lowest Viscosity Value Recorded = 6.45 cP

Therefore instrument error = ± 1.6%

The temperature was measured to within $0.1^{o}C$ (0.5% of lowest temperature encountered during experimentation).

Maximum error in measuring viscosity of suspending fluid = 2.1%

Particle Velocity

The distance between particle centres was measured to within 0.5 mm.

Smallest distance measured = 20 mm.

Error in Measuring a Distance Directly from the Screen = ± 2.5%

The magnification factor was obtained to within 1.8%.

Therefore maximum error in obtaining the distance travelled by a particle in time Δt = ± (2.5 1.8) = ± 4.3%

The error in Δt depends upon the error in filming speed. Figure 7 gives the setability in the regulated range as 5%. Values of V_{mean} obtained from particle velocity data were within 12% of the values given by the curve of figure 5.

Non-Dimensional Radial Coordinate of Particle Centre

The error in determining the radial position of particle centre, due to refraction of light at the liquid/glass interface, was estimated as < 1% of tube diameter (Appendix 6). Hence maximum error in n = ±2%.

Tube Diameters

Internal diameters were measured at the expansion end of the tube with the aid of vernier calipers (accuracy 0.001% per inch). The mean of three diameters was taken as the diameter d (Figure 3) and the out-of-roundness expressed as (largest diameter - smallest diameter) / mean. The largest value of this parameter was 0.6%.

APPENDIX 6

COMPUTER PROGRAM

The following program has been written in Fortan IV.

NOTATION

A	Eigenvalue, α_i
AN	Product of α_i and η
B	Coefficient of Non-Dimensional Input Profile, $\omega = f(\eta)$
C	Coefficient, c_i
D	Coefficient of Velocity Profile, $v_z = f(\eta)$
DENOM	Value of Denominator on Right Hand Side of Equation 2.11
DWDETA	First Derivative of ω with respect to η
DWDZ	First Derivative of ω with respect to Z^*
EDENOM	Leading Error Term Associated with Numerical Integration of FDENOM
ENVM	Leading Error Term Associated with Numerical Integration of FNVM
EPSIL	Stretching Factor, ϵ
ETA	Non-Dimensional Radial Coordinate, η
FDENOM	Expression under the Integral Sign in the Denominator of the Right Hand Side of Equation 2.11

NOTATION

G	Eigenfunction, g_i
VDENOM	Value of $2^{nd.}$ term in denominator of 2.11
VMEAN	Mean velocity, V_m
VNUM	Value of numerator of right hand side of equation 2.11
W	Non-dimensional Axial Velocity, ω
WFD	Fully Developed Velocity, $\omega_{f.d.}$
WSTAR	Non-dimensional Difference Velocity, ω^*
ZSTAR	Non-dimensional Axial Parameter which is a Function of the Stretched Coordinate, z^*
ZSTMAX	Maximum Value of Above Parameter

FLOW CHART

BOX NO.	COMMENTS
1	Input Parameters - Coefficients of v_z Polynomial and Maximum Value of Z* (corresponding to ω_c = 2.02 ± 0.00005)
2	Calculation of Coefficients of Non-dimensional Velocity Profile, $\omega = f(\eta)$
3	The first 100 eigenvalues, α_i, are calculated, together with the corresponding coefficients, c_i
4	The eigenfunctions, g_i, are computed from the above values of α_i and for η going from 0 to 1 in steps of 0.025.
5	ω is calculated for $Z^* \leq 0.005$ using first 100 terms in series $\Sigma\, c_i\, g_i\, e^{-\alpha_i^2 Z^*}$
6	ω is -alculated for $Z^* > 0.005$ using first 25 terms in above series (convergence is far more rapid now - taking more terms results in floating overflow)
7	Terms on right hand side of equation 2.11 are computed for $Z^* \leq 0.005$ using first 100 terms in corresponding series.
8	Terms on right hand side of equation 2.11 are computed for $Z^* > 0.005$ using first 25 terms in corresponding series.

BOX NO.	COMMENTS
9	21 values of ϵ are computed at equal intervals, H, from $Z^* = 0.0$ to $Z^* = Z^*_{MAX}$
10	Value of ϵ at $Z^* = 0.0$ is replaced by value at $Z^* = H/40$. (Slowness of convergence of series when $Z^* = 0.0$ generally leads to too large a value for ϵ)
11	Area under ϵ versus Z^* curve is found by numerical integration and the value of Z_{MAX} is printed.

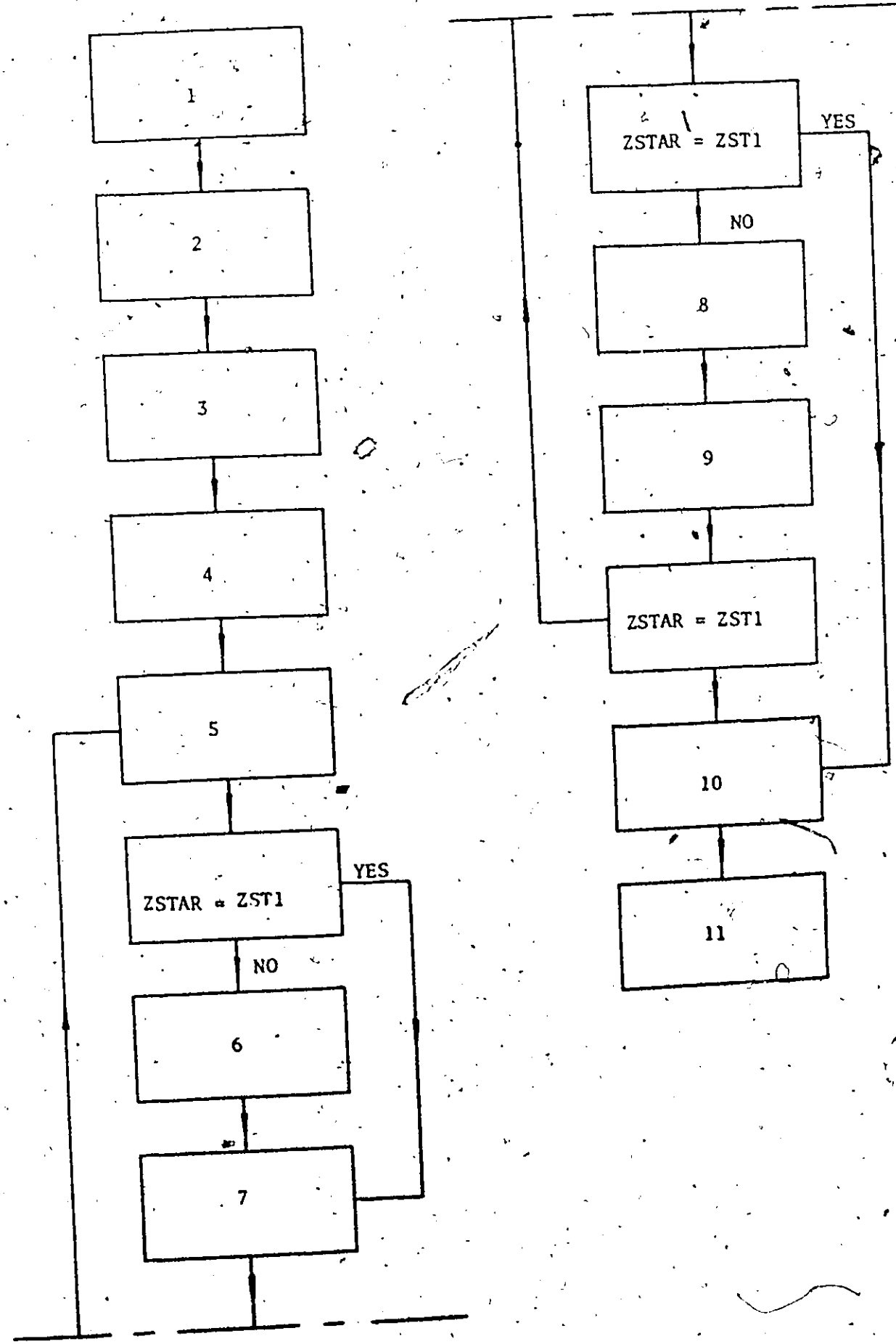
1
2
3
4
5
ZSTAR = ZST1
YES
NO
6
7
ZSTAR = ZST1
YES
NO
8
9
ZSTAR = ZST1
10
11

```
C     THE FIRST PART OF THE PROGRAM COMPUTES AND PRINTS THE VALUES
C     OF THE C COEFFICIENTS
      DIMENSION A(100),C(100),FIA(41),AN(100,41),B(7),D(7),
     *G(100,41),TERM(100,41),NED(41),STAR(41),W(20,41),DWDZ(20,41),
     *DWDETA(20,41),ATERM(100,41),BTERM(100,41),FNUM(20,41),FDENOM
     *(20,41),VNUM(20),FNUM(20),VDENOM(20),FDENOM(20),EPSIL(20),TERM1(2
     *),TERM2(20),DENOM(20),FA(100),DFA(100)
C     D(I) AND ZSTMAX ARE THE INPUT PARAMETERS
      ZSTMAX = 0.1451
      H = ZSTMAX*0.5E-01
      ZST1 = H/2.
      D(1) = 2.0971222
      D(2) = 0.0
      D(3) = -2.5480638
      D(4) = 0.0
      D(5) = 0.77419297
      D(6) = 0.0
      D(7) = -0.32325392
      SUM = D(1)/2.
      DO 15 K = 2,7
      J = K+1
      T = J
15    SUM = SUM+D(K)/T
      VMEAN = SUM*2.
      DO 5 I=1,7
5     B(I) = D(I)/VMEAN
      WRITE (6,300)
300   FORMAT (1H1,30X,4HA(I),35X,4HC(I),14X,4HIER0,2X,4HIER1)
      I=1
      A(1)=5.135620
1     CONTINUE
C     J-BESSEL FUNCTIONS OF ORDER 1 AND 2 ARE COMPUTED USING LIBRARY
C     SUBROUTINE BESJ
      CALL BESJ  (A(I),0,BJ0,1.0E-10,IER0)
      CALL BESJ  (A(I),1,BJ1,1.0E-10,IER1)
      BJ2 = 2./A(I)*BJ1-BJ0
      FA(I)=BJ1-(A(I)/2.0)*BJ0
      DFA(I)=0.5*(A(I)*BJ1-BJ2)
      A(I)=A(I)-FA(I)/DFA(I)
      IF (ABS(FA(I)/DFA(I)).GT.1.0E-10) GO TO 1
      C(I) = ((2.+B(3)+4.*B(5)/3.+1.5*B(7))/A(I))+((576.*B(7)/A(I)**2
     *     -48.*B(7)-16.*B(5))/A(I)**3)
      WRITE (6,3)  I,A(I),C(I),IER0,IER1
3     FORMAT  (1H0,15X,I2,3X,E18.10,20X,E18.10,5X,2(5X,I1))
      IF (I.GE.30) GO TO 4
      I=I+1
      A(I) = A(I-1)+3.14155
      GO TO 1
4     CONTINUE
C     FOR LARGE VALUES OF THE ARGUMENT,A(I),THE FUNCTION SUBPROGRAMS
C     SUB0 AND SUB1 ARE USED TO COMPUTE THE J-BESSEL FUNCTIONS
      BJ0 = SUB0(A(I))
      BJ1 = SUB1(A(I))
      BJ2 = 2./A(I)*BJ1-BJ0
      FA(I)=BJ1-(A(I)/2.0)*BJ0
      DFA(I)=0.5*(A(I)*BJ1-BJ2)
      A(I)=A(I)-FA(I)/DFA(I)
      IF (ABS(FA(I)/DFA(I)).GT.1.0E-08) GO TO 4
      C(I) = ((2.+B(3)+4.*B(5)/3.+1.5*B(7))/A(I))+((576.*B(7)/A(I)**2
```

```
*       -48.*P(7)-16.*P(5))/A(I)**3)
        WRITE (6,34) I,A(I),C(I),IER0,IER1
34      FORMAT (1H0,15X,I2,3X,E18.10,20X,E18.10,5X,2(5X,I1))
        IF (I.GE.100) GO TO 14
        I = I+1
        A(I) = A(I-1)+3.14155
        GO TO 4
14      CONTINUE
        SECOND PART OF PROGRAM GENERATES G(I,J) AS A FUNCTION OF A(I)
        AND ETA (J)
        DO 100 I = 1,100
        ETA(1)=0.0
        IERAN=0
        BJ0 = SUB0(A(I))
        IF (ABS(BJ0).LT.1.0E-06)STOP
        G(I,J)=(2./A(I))*(1./BJ0-1.)
        DO 10 J = 2,41
        ETA(J) = ETA(J-1)+0.025
        AN(I,J) = A(I)*ETA(J)
        IF (AN(I,J).GT.5.) GO TO 16
        CALL BESJ (AN(I,J),0,BJAN,1.0E-10,IERAN)
        GO TO 17
16      BJAN = SUB0(AN(I,J))
17      G(I,J)=(2.0/A(I))*(BJAN/BJ0-1.0)
10      CONTINUE
100     CONTINUE
        WSTAR AND W ARE COMPUTED AS A FUNCTION OF ETA FOR ZSTAR = 0.0
        TO ZSTAR(MAX)
        ZSTAR(MAX) CORRESPONDS TO W(CL) = 2.02 CORRECT TO 4 DEC. PLACES
        THE FIRST 100 TERMS IN THE SERIES ARE USED TO COMPUTE WSTAR
        UP TO ZSTAR = 0.005
        ZSTAR = 0.0
        K = 1
23      WRITE (6,26) ZSTAR
26      FORMAT (1H0,60X,6HZSTAR=F10.8//17X,3HETA,40X,5HWSTAR,40X,1HW)
        DO 25 J = 1,41
        THE FULLY DEVELOPED VELOCITY PROFILE IS COMPUTED
        WFD(J) = 2.*(1.-ETA(J)**2)
        WSTAR(J) = 0.0
        DO 24 I = 1,100
        IF (K-1) 12,2,12
2       TERM (I,J) = C(I)*G(I,J)
        GO TO 220
12      TERM (I,J) = C(I)*G(I,J)/EXP(A(I)**2*ZSTAR)
220     CONTINUE
24      WSTAR(J) = WSTAR(J) + TERM(I,J)
        W(K,J) = WFD(J) + WSTAR(J)
25      WRITE (6,27) ETA(J),WSTAR(J),W(K,J)
27      FORMAT (1H0,15X,F6.4,30X,E20.10,25X,E20.10)
        IF (ZSTAR.EQ.ZST1) GO TO 199
        ZSTAR = ZSTAR+H
        K = K+1
        IF (ZSTAR.LE.0.005) GO TO 23
33      CONTINUE
2222    WRITE (6,3333)ZSTAR
3333    FORMAT (1H0,60X,6HZSTAR=F10.8//17X,3HETA,40X,5HWSTAR,40X,1HW)
        DO 222 J = 1,41
        WSTAR(J) = 0.0
```

```
      THE FIRST 25 TERMS ARE NOW USED TO COMPUTE WSTAR
      DO 111 I = 1,25
      TERM(I,J) = C(I)*G(I,J)/EXP(A(I)**2*ZSTAR)
  111 WSTAR(J) = WSTAR(J)+TERM(I,J)
      W(K,J) = WED(J)+WSTAR(J)
  222 WRITE(6,227)ETA(J),WSTAR(J),W(K,J)
  227 FORMAT (1H0,15X,F6.4,30X,E20.10,25X,E20.10)
      ZSTAR = ZSTAR+H
      K = K+1
      IF (ZSTAR.LE.ZSTMAX) GO TO 33
      THE NEXT PART OF THE PROGRAM GENERATES THE RELATIONSHIP
      BETWEEN Z AND ZSTAR
      THE FIRST 100 TERMS ARE USED TO COMPUTE THE SERIES WHEN ZSTAR IS
      LESS THAN OR EQUAL TO 0.005
      ZSTAR = 0.0
      K = 1
  100 WRITE(6,202) ZSTAR
  202 FORMAT (1H1,60X,6HZSTAR=E10.8//2X,3HETA,12X,4HDWDZ,20X,6HDWDETA,
     1  20X, 4HFNUM,20X,6HFDENOM,12X,2HIO,3X,3HIAN,3X,4HIAN1)
      DO 62 J = 1,41
      DWDZ(K,J) = 0.0
      DWDETA (K,J) = -4.*ETA(J)
      DO 63 I = 1,100
      AN(I,1) = I.
      BJO = SUBO(A(I))
      IO = 0
      IF (AN(I,J).GT.5.)GO TO 18
      CALL BESJ  (AN(I,J),0,BJAN,1.0E-10,IAN)
      CALL BESJ  (AN(I,J),1,BJ1AN,1.0E-10,IAN1)
      GO TO 19
   18 BJAN = SUBO(AN(I,J))
      BJ1AN = SUB1(AN(I,J))
   19 IF (J-1) 120,20,120
   20 IAN = 0
      BJAN = 1.0
      IAN1 = 0
      BJ1AN = 0.0
  120 CONTINUE
      IF (K-1) 140,40,140
   40 ATERM (I,J) = 2.*C(I)*A(I)*(BJO-BJAN)/BJO
      BTERM (I,J) = -2.*C(I)*BJ1AN/BJO
      GO TO 240
  140 ATERM (I,J) = 2.*C(I)*A(I)*(BJO-BJAN)/(BJO*EXP(A(I)**2*ZSTAR))
      BTERM(I,J) = -2.*C(I)*BJ1AN/(BJO*EXP(A(I)**2*ZSTAR))
  240 CONTINUE
      DWDZ(K,J) = DWDZ(K,J)+ATERM(I,J)
   63 DWDETA(K,J) = DWDETA(K,J)+BTERM(I,J)
      FNUM(K,J) = (5.-W(K,J)-1.5*(K,J)**2)*DWDZ(K,J)*ETA(J)
      FDENOM(K,J) = ETA(J)*DWDETA(K,J)**2
   63 WRITE(6,203) ETA(J),DWDZ(K,J),DWDETA(K,J),FNUM(K,J),
     1FDENOM(K,J),IO,IAN,IAN1
  203 FORMAT (1H0,F6.4,4(5X,E20.10),3(5X,I1))
      IF(ZSTAR.EQ.ZST1) GO TO 1005
      ZSTAR = ZSTAR+H
      K = K+1
      IF (ZSTAR.LE.0.005) GO TO 100
  333 CONTINUE
 4444 WRITE (6,5555) ZSTAR
```

```
5555 FORMAT (1H1,60X,6HZSTAR=F10.8//2X,3HETA,12X,4HDWDZ,20X,6HDWDETA,
     1    20X,4HENUM,20X,6HFDENOM,12X,2HI0,3X,3HIAN,3X,4HIAN1)
     ONLY THE FIRST 25 TERMS ARE NOW TAKEN IN COMPUTING THE SERIES
      DO 662 J = 1,41
      DWDZ(K,J) = 0.0
      DWDETA(K,J) = -4.*ETA(J)
      DO 663 I = 1,25
      BJ0 = SUB0(A(I))
      IF (AN(I,J).GT.5.) GO TO 28
      CALL BESJ (AN(I,J),0,BJAN,1.0E-10,IAN)
      CALL BESJ (AN(I,J),1,BJ1AN,1.0E-10,IAN1)
      GO TO 29
   28 BJAN = SUB0 (AN(I,J))
      BJ1AN = SUB1 (AN(I,J))
   29 CONTINUE
      IF (J-1) 150,50,150
   50 IAN = 0
      BJAN = 1.0
      IAN1 = 0
      BJ1AN = 0.0
  150 CONTINUE
      ATERM (I,J) = 2.*C(I)*A(I)*(BJ0-BJAN)/(BJ0*EXP(A(I)**2*ZSTAR))
      BTERM (I,J) = -2.*C(I)*BJ1AN/(BJ0*EXP(A(I)**2*ZSTAR))
      DWDZ (K,J) = DWDZ(K,J)+ATERM(I,J)
  663 DWDETA (K,J) = DWDETA(K,J)+BTERM(I,J)
      FNUM(K,J) = (2.*W(K,J)-1.5*W(K,J)**2)*DWDZ(K,J)*ETA(J)
      FDENOM(K,J) = ETA(J)*DWDETA(K,J)**2
  662 WRITE (6,222) ETA(J),DWDZ(K,J),DWDETA(K,J),FNUM(K,J),
     1    FDENOM(K,J),I0,IAN,IAN1
  222 FORMAT (1H0,F6.4,4(5X,E20.10),3(5X,I1))
      ZSTAR = ZSTAR+H
      K = K+1
      IF (ZSTAR.LE.ZSTMAX) GO TO 333
C     THE NEWTON-COTES 4 STRIP, 5 POINT INTEGRATION FORMULA IS USED
C     TO COMPUTE VNUM AND VDENOM
      WRITE (6,176)
  176 FORMAT (1H1,13X,4HVNUM,21X,4HFNUM,20X,6HVDENOM,19X,6HFDENOM,
     1    20X,6HEPSIL)
      DO 105 K = 1,21
      TERM1(K) = 0.0
      DO 174 N = 1,37,4
  174 TERM1(K) = TERM1(K)+7.*FNUM(K,N)+32.*FNUM(K,N+1)+12.*FNUM(K,N+2)
     1    +32.*FNUM(K,N+3)+7.*FNUM(K,N+4)
      VNUM(K) = TERM1(K)/90.
C     AN ESTIMATE OF THE LEADING ERROR TERM IS ALSO OBTAINED
      FNUM(K) = ABS(2.*(FNUM(K,24)-6.*FNUM(K,23)+15.*FNUM(K,22)
     1    -20.*FNUM(K,21)+15.*FNUM(K,20)-6.*FNUM(K,19)+FNUM(K,18))/945.)
      TERM2(K) = 0.0
      DO 175 N = 1,37,4
  175 TERM2(K) = TERM2(K)+7.*FDENOM(K,N)+32.*FDENOM(K,N+1)+12.*
     1    FDENOM(K,N+2)+32.*FDENOM(K,N+3)+7.*FDENOM(K,N+4)
      VDENOM(K) = TERM2(K)/90.
      DENOM(K) = DWDETA(K,41)+VDENOM(K)
      FDENOM(K)=ABS(2.*(FDENOM(K,24)-6.*FDENOM(K,23)+15.*FDENOM(K,22)
     1    -20.*FDENOM(K,21)+15.*FDENOM(K,20)-6.*FDENOM(K,19)+FDENOM(K,18)
     1    )/945.)
      EPSIL(K) = VNUM(K)/DENOM(K)
  105 WRITE (6,177) K,VNUM(K),FNUM(K),VDENOM(K),FDENOM(K),EPSIL(K)
```

```
177   FORMAT (1H0,I2,3X,4(E20.10,5X),E20.10)
      K = 22
      ZSTAR = ZST1
      GO TO 23
1066  TERM1(K) = 0.0
      DO 1740 N = 1,37,4
1740  TERM1(K) = TERM1(K)+7.*FNUM(K,N)+32.*FNUM(K,N+1)+12.*FNUM(K,N+2)
     1    +32.*FNUM(K,N+3)+7.*FNUM(K,N+4)
      VNUM(K) = TERM1(K)/900.
      AN ESTIMATE OF THE LEADING ERROR TERM IS ALSO OBTAINED
      FNUM(K) = ABS(2.*(FNUM(K,24)-6.*FNUM(K,23)+15.*FNUM(K,22)
     1   -20.*FNUM(K,21)+15.*FNUM(K,20)-6.*FNUM(K,19)+FNUM(K,18))/945.)
      TERM2(K) = 0.0
      DO 1750 N = 1,37,4
1750  TERM2(K) = TERM2(K)+7.*FDENOM(K,N)+32.*FDENOM(K,N+1)+12.*
     1   FDENOM(K,N+2)+32.*FDENOM(K,N+3)+7.*FDENOM(K,N+4)
      VDENOM(K) = TERM2(K)/900.
      DENOM(K) = DWDETA(K,41)+VDENOM(K)
      FDENOM(K)=ABS(2.*(FDENOM(K,24)-6.*FDENOM(K,23)+15.*FDENOM(K,22)
     1   -20.*FDENOM(K,21)+15.*FDENOM(K,20)-6.*FDENOM(K,19)+FDENOM(K,18)
     1    )/945.)
      EPSIL(K) = VNUM(K)/DENOM(K)
1050  WRITE (6,1770) K,VNUM(K),ENUM(K),VDENOM(K),EDENOM(K),EPSIL(K)
1770  FORMAT (1H0,I2,2X,4(E20.10,5X),E20.10)
      EPSIL(1) = EPSIL(22)
C     THE VALUE OF ZMAX IS NOW OBTAINED BY NUMERICALLY INTEGRATING
C     UNDER THE CURVE OF EPSILON VS. ZSTAR
      TERM3 = 0.0
      DO 123 K = 1,19,2
123   TERM3 = TERM3+EPSIL(K)+4.*EPSIL(K+1)+EPSIL(K+2)
      ZMAX = TERM3*2.*H/45.
      WRITE (6,234) ZMAX
234   FORMAT (1H0,50X,4HZMAX//40X,E20.10)
      END
C     THE FOLLOWING FUNCTION SUBPROGRAMS APPLY ONLY FOR A VALUE OF X
C     EQUAL TO OR GREATER THAN 3.
      FUNCTION SUB0 (X)
      DIMENSION A(10)
      I = 1
      A(I) = X
      F0 = 0.797884566-0.00000077*(3./A(I))-0.00552740*(3./A(I))**2
     *   -0.00009512*(3./A(I))**3+0.00137237*(3./A(I))**4-0.00072805*
     *   (3./A(I))**5+0.00014476*(3./A(I))**6
      THETA0 = A(I)-.785398163-.04166397*(3./A(I))-.00003954*(3./A(I))**2
     *    +.00262573*(3./A(I))**3-.00054125*(3./A(I))**4-.00029333*
     *   (3./A(I))**5+.00013558*(3./A(I))**6
      SUB0 = F0*COS(THETA0)/SQRT(A(I))
      RETURN
      END
      FUNCTION SUB1 (X)
      DIMENSION A(10)
      I = 1
      A(I) = X
      F1 = .797884566+.00000156*(3./A(I))+.01659667*(3./A(I))**2
     *    +.00187118*(3./A(I))**3-.00250541*(3./A(I))**4+.00113653*
     *   (3./A(I))**5-.00020033*(3./A(I))**6
      THETA1 = A(I)-2.356194490+.12499612*(3./A(I))+.00005650*(3./A(I))
     *   **2-.00637879*(3./A(I))**3+0.00074348*(3./A(I))**4+
```

```
*    0.0+0.0+0.0+
```

APPENDIX 7

TABULATED EXPERIMENTAL DATA

TABLES 5 - 10

STATION I		STATION 2	
r/R	v_z (cm./sec.)	r/R	v_z (cm/sec.)
0.23876	15.4290	0.41498	12.8570
0.83086	4.04760	0.45677	12.2860
0.85675	3.57140	0.76226	6.57140
0.83789	4.07140	0.71723	7.67860
0.83157	4.48980	0.71949	7.42860
0.83481	4.15580	0.61414	9.2857
0.85186	3.49210	0.74912	6.78570
0.18595	16.6670	0.91871	2.41760
0.83170	3.96100	0.74701	6.42860
0.19307	16.6670	0.64701	8.57140
0.33187	13.8100	0.38744	12.8570
0.41437	12.8570	0.89613	3.17460
0.75852	5.71430	0.83211	4.95240
0.73843	6.07140	0.58977	9.79590
0.81732	4.28570	0.83643	4.76190
0.91558	2.46750	0.42837	12.3810
0.16555	17.4290	0.83423	4.64290
0.58499	9.52380	0.69756	7.6190
		0.88276	3.92860
		0.63331	9.28570
		0.70684	7.8571
		0.34089	14.0820
		0.22116	15.0000

TABLE 3 VELOCITY DATA FOR EXPERIMENT A1

STATION 1		STATION 2	
r/R	v_z (cm/sec.)	r/R	v_z (cm/sec.)
0.50533	20.8330	0.43171	26.6670
0.31739	33.0000	0.78451	9.6875
0.39306	27.5000	0.59148	20.0000
0.58801	15.2780	0.71870	13.0770
0.36207	31.8750	0.40092	29.3750
0.61866	13.4380	0.48162	25.7140
0.14520	56.2500	0.60644	18.0000
0.38113	32.5000	0.68536	14.5000
0.18089	48.3330	0.75067	10.0000
0.52336	17.9170	0.64993	14.0000
0.083157	58.7500	0.57533	19.5000
0.23059	47.5000	0.22811	37.5000
0.47788	21.5000	0.29870	35.8330
0.61170	12.5000	0.13052	41.6670
0.45455	23.7500	0.71440	14.3750
0.80721	3.1944	0.87064	5.8333
0.62368	12.1430		
0.85835	3.01470		
0.77849	7.8125		
0.72221	7.0833		
0.58801	16.2500		
0.33691	36.6670		
0.36756	31.2500		
0.098265	57.5000		
0.60372	14.5830		
0.50403	20.8330		
0.038961	58.0000		
0.82842	4.7059		

TABLE 4 VELOCITY DATA FOR EXPERIMENT A2

STATION I		STATION 2	
r/R	v_z (cm/sec)	r/R	v_z (cm/sec.)
0.36300	19.4290	0.68259	12.2860
0.81000	7.45340	0.18089	22.8570
0.51952	16.0000	0.55651	16.4290
0.54025	15.7140	0.89566	6.25000
0.48192	16.7860	0.37421	20.5710
0.87267	5.35710	0.087361	22.8570
0.34342	20.0000	0.81280	8.85710
0.75559	9.10710	0.20779	22.8570
0.63603	13.0950	0.86268	6.34920
0.63640	13.1430	0.89770	5.19480
0.26528	21.0710	0.38662	19.6430
0.11507	23.5710	0.57158	15.5840
0.67147	12.3810	0.55742	16.0000
0.38580	19.6830	0.41741	20.4760
0.54515	15.4760	0.34714	20.0000
0.514-1	16.0710	0.070238	23.8100
0.87662	5.32470	0.55737	15.7140
0.37104	20.4080	0.43171	18.3670
0.70803	11.0480	0.57334	16.4290
0.30291	21.0710	0.86087	6.15380
0.098265	23.5710	0.35714	20.0000
0.74932	9.52380	0.42283	19.2860
0.00000	23.8100	0.91215	5.05490
		0.58442	16.1900
		0.75576	10.1590
		0.84665	7.42860
		0.012987	23.5710

TABLE 5 VELOCITY DATA FOR EXPERIMENT B1

STATION 1		STATION 2	
r/R	v_z (cm/sec.)	r/R	v_z (cm/sec.)
0.54177	21.8750	0.75361	14.1670
0.44327	26.8750	0.60783	19.0000
0.58571	20.0000	0.34342	28.1250
0.60414	19.1670	0.55980	21.0000
0.32758	30.8330	0.88321	6.7500
0.82743	8.9583	0.14286	32.8570
0.68253	17.5000	0.67723	17.5000
0.20749	36.0000	0.42372	26.2500
0.80864	10.4170	0.74701	14.0000
0.58962	20.0000	0.73766	14.1670
0.51610	22.5000	0.62243	18.7500
0.83081	9.1667	0.43171	26.0000
0.67185	16.5000	0.19307	33.3333
0.86841	7.1875	0.86714	7.81250
0.73517	13.5000	0.17290	32.5000
0.79978	10.2780	0.43117	26.0000
0.72832	13.7500	0.89380	6.8750
0.76681	12.0830	0.25258	32.5000
0.10807	38.3330	0.26750	31.4290
0.12252	39.0000	0.15435	32.0000
0.04158	38.7500	0.83844	9.28570
0.09297	38.0000	0.74661	15.0000
0.26631	33.3330	0.071429	34.3750
0.30130	31.4290	0.73120	14.5830
0.09740	40.0000	0.28512	30.0000

TABLE 6 VELOCITY DATA FOR EXPERIMENT B2

STATION 1		STATION 2	
r/R	v_z (cm/sec.)	r/R	v_z (cm/sec.)
0.86256	9.32330	0.29983	43.8100
0.69699	19.0480	0.86792	10.0000
0.31845	44.5710	0.91844	7.39500
0.60166	25.1430	0.10081	55.2380
0.13387	57.1430	0.68456	21.7140
0.57276	26.8570	0.30712	45.7140
0.52613	31.0200	0.74245	20.0000
0.56925	27.9370	0.50152	33.1430
0.62598	24.0000	0.44199	38.5710
0.83930	10.4760	0.67257	22.8570
0.62080	24.4160	0.33288	42.8570
0.45994	37.1430	0.17156	51.4290
0.57147	28.0000	0.81117	14.6430
0.16883	57.1430	0.44725	35.7140
0.77273	16.2860	0.61770	25.4550
0.34071	43.8100	0.67981	21.7140
0.58499	28.5710	0.49491	33.3330
0.68182	18.7760	0.86490	10.7140
0.43681	37.1430	0.23947	52.3810
0.55575	26.8570	0.81944	13.3330
0.14991	57.1430	0.64210	23.5710
0.81689	10.8570	0.14991	53.7140
0.48266	33.5710	0.55712	29.3880
0.58719	25.7140	0.35358	41.9050
0.11616	57.1430	0.63067	25.4550
0.87593	7.77140	0.84578	11.4290
		0.74052	18.0950
		0.67663	21.9050

TABLE 7 VELOCITY DATA FOR EXPERIMENT B3

STATION 1		STATION 2
r/R	v_z (cm/sec.)	
0.87489	6.55460	
0.75663	10.4760	
0.69417	12.8570	
0.56765	17.1430	
0.88321	5.89290	
0.60292	15.0000	
0.49708	18.8570	
0.80648	8.28570	
0.51031	19.2860	
0.25974	23.1430	
0.25216	24.0000	
0.65931	13.0360	
0.46409	19.7140	
0.54332	17.9460	
0.88321	6.10710	
0.16695	23.8390	
0.41726	20.5710	
0.72765	10.7140	
0.68972	12.3210	
0.78192	11.3270	
0.75518	10.7140	

TABLE 8 VELOCITY DATA FOR EXPERIMENT C1

STATION 1		STATION 2	
r/R	v_z (cm/sec.)	r/R	v_z (cm/sec.)
0.70265	17.4110	0.79245	11.4290
0.24131	33.9290	0.44089	26.3390
0.62544	20.5360	0.70325	17.1430
0.93482	7.50000	0.19631	33.0360
0.89330	7.58930	0.27740	31.2500
0.35215	31.2500	0.29163	29.7620
0.49098	25.0000	0.77371	15.0000
0.69027	17.8570	0.65081	22.3210
0.69371	17.8570	0.49167	28.5710
0.36698	29.4640	0.28843	29.1670
0.063954	37.50000	0.77371	15.0000
0.65401	20.9820	0.59532	23.2140
0.54048	23.8100	0.40888	28.5710
0.73766	15.1790	0.84478	9.09090
0.49167	27.3810	0.27094	32.1430
0.50940	25.0000	0.58152	21.8750
0.66996	18.3040	0.53346	23.2140
0.71635	16.7860	0.66532	19.1960
0.69711	17.5000	0.75016	15.3060
0.25974	33.9290	0.30547	30.3570
0.78700	14.8810	0.40370	29.4640
0.73388	15.0000	0.44099	26.7860
0.74687	14.2860	0.36762	29.7620
0.18876	35.7140	0.55176	24.1070
0.84468	9.37500	0.59094	22.6190
		0.40165	28.5710
		0.65588	22.0240
		0.42108	28.1250
		0.84408	10.0000

TABLE 9 VELOCITY DATA FOR EXPERIMENT C2

STATION 1		STATION 2	
r/R	v_z (cm/sec.)	r/R	v_z (cm/sec.)
0.42452	34.2860	0.37217	38.5710
0.75173	18.2860	0.51377	31.4290
0.89037	9.52380	0.64935	24.4900
0.88333	8.80950	0.48822	33.4690
0.69611	20.5710	0.29451	41.9050
0.61743	24.4900	0.27990	39.1840
0.48680	30.8570	0.78794	16.7620
0.12791	44.0820	0.56288	28.5710
0.64613	25.1430	0.19481	42.4490
0.55651	29.3880	0.72614	20.0000
0.63577	24.0820	0.22681	41.9050
0.78528	16.1340	0.89077	9.25170
0.23520	41.4290	0.13698	43.5710
0.81850	14.1180	0.24641	43.4290
0.071429	45.0790	0.34878	40.9520
0.74245	18.5710	0.66634	23.6730
0.24244	40.7140	0.45570	33.5710
0.36364	38.0950	0.56702	28.0000
0.22087	43.4290	0.29983	39.2860
0.38983	36.1900	0.54064	30.0000
0.62503	27.4290	0.13698	44.2860
		0.79645	16.3270
		0.86969	10.1100
		0.77732	16.5080

TABLE 10 VELOCITY DATA FOR EXPERIMENT C3